

***Supporting Information (Part 1) for***  
**Structures, Rugged Energetic Landscapes, and**  
**Nanothermodynamics of  $\text{Al}_n$  ( $2 \leq n \leq 65$ ) Particles**

Zhen Hua Li, Ahren W. Jasper, Donald G. Truhlar  
*Department of Chemistry and Supercomputing Institute,*  
*University of Minnesota, Minneapolis, MN 55455-0431*

Supporting information for an article in *Journal of the American Chemical Society*

Date on which supporting information was prepared: May 3, 2007

Total number of pages; including this page: 50

***Contents***

Computational details	S2
References	S6
Additional nanothermodynamic equations	S7
Additional discussion	S9
Table S1	S13
Table S2	S14
Table S3	S17
Table S4	S20
Table S5	S23
Figures captions	S26
Figures S1–S8	S27

### ***Computational details***

***Potential energy function.*** The NP-B analytic potential energy function<sup>1</sup> is used throughout this article. This potential energy function is based on the embedded atom model of Mei and Davenport,<sup>2</sup> which was reparametrized and validated<sup>1</sup> for pure Al clusters and nanoparticles using a large and diverse dataset of density functional theory structures and energies.

***Big-bang (BB) searching algorithm.*** For each particle size  $n$ , 10,000 highly compressed nearly spherical particles were randomly generated, such that the minimum and maximum distances between any two nearest-neighbor atoms were 0.8 Å and 1.0 Å, respectively. Comparing these values to the experimental equilibrium bond distances in Al<sub>2</sub> (2.7 Å<sup>3</sup>) and bulk Al (2.8 Å) shows that the resulting structures are compressed to only ~4% of their equilibrium volumes. Each of the randomly generated clusters was then optimized using the Broyden-Fletcher-Goldfarb-Shanno (BFGS) algorithm<sup>4</sup> with a convergence criterion of  $5 \times 10^{-4}$  eV/Å for the maximum absolute value of the  $3N$  Cartesian gradient components. The lowest-energy structure in the resulting distribution of local minima for each  $n$  is denoted the big-bang global minimum (BBGM).

Many of the local minima that are found correspond to the same structure, and energetic and geometric criteria were used to determine the final set of distinct local minima. Specifically, two structures were deemed to be identical if (1) their energies differed by less than 0.01 eV and (2) no bond distance less than 5.4 Å (twice the bond distance in Al<sub>2</sub>) differed by more than 0.0005 Å.

***Molecular dynamics simulation and quenching (MDSQ) method.*** Molecular dynamics (MD) simulations were also performed for each cluster size  $n$ . In these simulations, a normal mode analysis was carried out at the BBGM, and 10 independent trajectories were started from the BBGM with the initial coordinates and momenta for each trajectory selected from a phase space distribution of classical harmonic oscillators<sup>5</sup> with a temperature of 200 K. The system was equilibrated at 200 K for 1.2 ns. The temperature was then increased by 20 K by raising the target temperature of the thermostat, and another 1.2 ns constant temperature simulation was performed. This heating was repeated until the temperature reached 1000 K for  $n > 30$  and 1400 K for  $n \leq 30$ . During the MD simulations, one out of every 1000 molecular configurations was randomly

quenched to the nearest local minimum. For nanoparticles with  $n > 30$ , an average of 246,000  $\left( = 10 \times \left( \frac{1000 - 200}{20} + 1 \right) \times \frac{1.2 \times 10^6}{2} \times \frac{1}{1000} \right)$  configurations were quenched, while for the smaller clusters, an average of 366,000  $\left( = 10 \times \left( \frac{1400 - 200}{20} + 1 \right) \times \frac{1.2 \times 10^6}{2} \times \frac{1}{1000} \right)$  configurations were quenched. Thus approximately  $1.9 \times 10^6$  configurations are quenched.

The molecular dynamics simulations were carried out using the Liouville formulation<sup>6</sup> of the velocity Verlet integrator<sup>7</sup> with a time step of 2.0 fs coupled with a two chain Nosé-Hoover thermostat.<sup>8,9</sup> The temperature of the particle is calculated using<sup>5</sup>

$$T = \frac{\sum_i \frac{p_i^2}{2m_i}}{\frac{1}{2} k_B N_f}, \quad (\text{A1})$$

where  $N_f$  is the number of degrees of freedom of the particle, and  $k_B$  is the Boltzmann constant.

The molecular dynamics program used was ANT 07.<sup>10</sup>

A set of distinct local minima was obtained from the quenched structures using the energetic and geometric criteria discussed above. We note that if more than 2000 distinct minima were found, only the 2000 lowest-energy ones were considered.

For  $n < 50$ , both the BB and the MDSQ methods found the same lowest-energy minima. For some nanoparticles with  $n \geq 50$ , the lowest-energy minimum located by the BB method is 0.2 – 0.3 eV higher in energy than that located by the MDSQ simulations. The total number of distinct minima located by the BB algorithm is much larger than that of the MDSQ algorithm. For example, more than 1000 distinct minima were located for particles larger than  $\text{Al}_{16}$  using the BB method, whereas only 571, 496, and 535 structures are located using the MDSQ simulations for  $\text{Al}_{19}$ ,  $\text{Al}_{20}$ , and  $\text{Al}_{21}$ , respectively. Despite these differences, there is generally good agreement among the sets of structures (isomers) located by the two searching methods, so we believe that the structures obtained are complete enough to draw conclusions about energy landscapes, magic numbers, and average isomeric energies. When calculating  $P_\gamma$  or  $P_\gamma^{\text{FS}}$ , the sum in Eqs. 5 and 6 is over all (2000 at

most) lowest-energy isomers determined in the MDSQ step (except for  $\text{Al}_2$  and  $\text{Al}_3$ , which are treated as special cases).

**Partition functions.** The rotational partition function of isomer  $\gamma$  is calculated by the classical rigid-rotor approximation, which yields

$$q_{\text{Rot}}^{(\gamma)} = \left( \frac{8\pi^2 k_B T}{h^2} \right)^{3/2} \frac{\sqrt{\pi A^{(\gamma)} B^{(\gamma)} C^{(\gamma)}}}{\sigma^{(\gamma)}}, \quad (\text{A2})$$

for non-linear structures, where  $A^{(\gamma)}$ ,  $B^{(\gamma)}$ , and  $C^{(\gamma)}$  are the three principal moments of inertia and  $\sigma^{(\gamma)}$  is the rotational symmetry number, and yields

$$q_{\text{Rot}}^{(\gamma)} = \frac{8\pi^2 I^{(\gamma)} k_B T}{\sigma^{(\gamma)} h^2}, \quad (\text{A3})$$

for linear structures, where  $I^{(\gamma)}$  is the moment of inertia. To obtain  $\sigma^{(\gamma)}$ , one needs to know the point group symmetry of every isomer. This is found using *Gaussian 03*<sup>62</sup> (with a “loose” criterion for judging the symmetry of molecules, i.e., keyword `symm=loose`). The vibrational partition function is calculated using the harmonic-oscillator approximation,

$$q_{\text{Vib}}^{(\gamma)} = \prod_m \frac{e^{-h\omega_m^{(\gamma)}/2k_B T}}{1 + e^{-h\omega_m^{(\gamma)}/k_B T}}, \quad (\text{A4})$$

where  $\omega_m^{(\gamma)}$  is the harmonic vibrational frequency of mode  $m$  of isomer  $\gamma$ .

One problem of calculating  $q_{\text{Vib}}^{(\gamma)}$  using Eq. A4 is that, for the large particles, there are many low-frequency vibrational modes. These small frequencies make very large contributions that are proportional in the classical limit to the reciprocal of the frequency. However,  $q_{\text{Vib}}^{(\gamma)}$  calculated using either Eq. 11 or this low-frequency limit may be overestimated because of the anharmonicity of the vibration. To reduce the error caused by the breakdown of the harmonic approximation for small frequencies, one may raise all the small frequencies (those that are below a certain value); for example, one may raise all frequencies smaller than  $100 \text{ cm}^{-1}$  to  $100 \text{ cm}^{-1}$ .

This produces an independent-mode effective harmonic oscillator whose statistical thermodynamic properties better mimic those of the anharmonic low-frequency coupled mode. We tested three values,  $70 \text{ cm}^{-1}$ ,  $100 \text{ cm}^{-1}$ , and  $130 \text{ cm}^{-1}$ , for the cutoff frequency. The nonseparable distributions calculated using the three values are not very different, for example, the average absolute deviation (average over all 64 particles) of the probabilities of the global minimum at 1500 K calculated using  $100 \text{ cm}^{-1}$  to those probabilities calculated using  $70 \text{ cm}^{-1}$  and  $130 \text{ cm}^{-1}$  are just 7 and 4 percent, respectively. Therefore, we somewhat arbitrarily choose  $100 \text{ cm}^{-1}$ .

Although the harmonic-oscillator, rigid-rotator motor is not appropriate for the most quantitative work on small molecules, it is chosen because its efficiency allows the calculation of the required large number ( $\sim 10^5$ ) of rovibrational partition functions of these often very large molecules (average number of frequencies  $\sim 10^2$ ). With the above effective-frequency treatment of low-frequency modes, it should be accurate enough for studying the distribution properties of the isomers.

In evaluating Eq. 17 we assume in this article that  $q_{\text{Elec}}$  is independent of  $n$ .

**Density of vibrational states.** The expansion in Legendre polynomials  $P_\ell(\omega)$  is truncated at  $\ell_{\text{max}} = 30$ .

**Units.**  $1 \text{ eV/particle} = 23.6 \text{ kcal/mol} = 96.5 \text{ kJ/mol}$ .

## References

- <sup>1</sup>Jasper, A. W.; Schultz, N. E.; Truhlar, D. G. *J. Phys. Chem. B* **2005**, *109*, 3915.
- <sup>2</sup>J. Mei and J. W. Davenport, *Phys. Rev. B* **1992**, *46*, 21.
- <sup>3</sup>Fu, Z. W.; Lemire, G. W.; Bishea, G. A.; Morse, M. D. *J. Chem. Phys.* **1990**, *93*, 8420.
- <sup>4</sup>Broyden, C. G. *J. I. Math. App.* 1970, *6*, 76-90; Fletcher, R. *Comput. J.* **1970**, *13*, 317; Goldfarb, D. *Math. Comput.* **1970**, *24*, 23; Shanno, D. F. *Math. Comput.* **1970**, *24*, 647.
- <sup>5</sup>Peslherbe, G. H.; Hase, W. L. *J. Chem. Phys.* **1994**, *101*, 8535.
- <sup>6</sup>Frenkel, D.; Smit, B. *Understanding Molecular Simulation: From Algorithms to Applications*; Academic Press: San Diego, 2002.
- <sup>7</sup>Swope, W. C.; Andersen, H. C.; Berens, P. H.; Wilson, K. R. *J. Chem. Phys.* **1982**, *76*, 637.
- <sup>8</sup>Nosé, S. *J. Chem. Phys.* 1984, *81*, 511; Nosé, S. *Mol. Phys.* 1984, *52*, 255.
- <sup>9</sup>Martyna, G. J.; Klein, M. L.; Tuckerman, M. E. *J. Chem. Phys.* **1992**, *97*, 2635.
- <sup>10</sup>Li, Z. H.; Jasper, A. W.; Bonhommeau, D. A.; Truhlar, D. G. *ANT 07*; University of Minnesota: Minneapolis, 2007.
- <sup>11</sup>Frisch, M. J.; Trucks, G. W.; Schlegel, H. B.; Scuseria, G. E.; Robb, M. A.; Cheeseman, J. R.; Montgomery, Jr., J. A.; Vreven, T.; Kudin, K. N.; Burant, J. C.; Millam, J. M.; Iyengar, S. S.; Tomasi, J.; Barone, V.; Mennucci, B.; Cossi, M.; Scalmani, G.; Rega, N.; Petersson, G. A.; Nakatsuji, H.; Hada, M.; Ehara, M.; Toyota, K.; Fukuda, R.; Hasegawa, J.; Ishida, M.; Nakajima, T.; Honda, Y.; Kitao, O.; Nakai, H.; Klene, M.; Li, X.; Knox, J. E.; Hratchian, H. P.; Cross, J. B.; Bakken, V.; Adamo, C.; Jaramillo, J.; Gomperts, R.; Stratmann, R. E.; Yazyev, O.; Austin, A. J.; Cammi, R.; Pomelli, C.; Ochterski, J. W.; Ayala, P. Y.; Morokuma, K.; Voth, G. A.; Salvador, P.; Dannenberg, J. J.; Zakrzewski, V. G.; Dapprich, S.; Daniels, A. D.; Strain, M. C.; Farkas, O.; Malick, D. K.; Rabuck, A. D.; Raghavachari, K.; Foresman, J. B.; Ortiz, J. V.; Cui, Q.; Baboul, A. G.; Clifford, S.; Cioslowski, J.; Stefanov, B. B.; Liu, G.; Liashenko, A.; Piskorz, P.; Komaromi, I.; Martin, R. L.; Fox, D. J.; Keith, T.; Al-Laham, M. A.; Peng, C. Y.; Nanayakkara, A.; Challacombe, M.; Gill, P. M. W.; Johnson, B.; Chen, W.; Wong, M. W.; Gonzalez, C.; and Pople, J. A.; *Gaussian 03*, Revision C.02; Gaussian, Inc.: Wallingford , CT, 2004.

### ***Additional nanothermodynamic equations***

Assuming separable electronic, vibrational, and rotational motions, Eq. 18 becomes

$$\Delta E_T^{\text{tot}} = 1.5kT + E_T^{\text{Elec}} + \sum_{\gamma} (\Delta E_e^{(\gamma)} + E_{\text{Vib}}^{(\gamma)} + E_{\text{Rot}}^{(\gamma)}) P_{\gamma}, \quad (\text{B1})$$

where  $E_{\text{Vib}}^{(\gamma)}$  and  $E_{\text{Rot}}^{(\gamma)}$  are the vibrational energy and rotational energy of isomer  $\gamma$ , respectively.

In the classical limit,  $E_{\text{Rot}}^{(\gamma)} = 1.5kT$  for non-linear particles and  $E_{\text{Rot}}^{(\gamma)} = kT$  for linear particles. The energy of the particle including thermal and ZPE contributions is then given by

$$E_T^{\text{tot}} = E_e^{(1)} + \Delta E_T^{\text{tot}}. \quad (\text{B2})$$

Note that  $E_{\text{Vib}}^{(\gamma)}$  and  $\Delta E_T^{\text{tot}}$  include ZPE.

Most work on clusters and nanoparticles focuses on the energetics of the global minima; thermal and ZPE contributions are often neglected. It is interesting to compare conclusions based on the classical equilibrium energies of the global minima to those based on the thermal average energies in which both ZPE and thermal contributions are included. Thus we define

$$\Delta_1 E_T^{\text{tot}}(n) = [E_T(1) + E_T^{\text{tot}}(n-1)] - E_T^{\text{tot}}(n), \quad (\text{B3})$$

$$\Delta_2 E_T^{\text{tot}}(n) = E_T^{\text{tot}}(n-1) + E_T^{\text{tot}}(n+1) - 2E_T^{\text{tot}}(n), \quad (\text{B4})$$

At 0 K and excluding ZPE contributions, these quantities will reduce to  $\Delta_1 E_e^{(1)}(n)$  or  $\Delta_2 E_e^{(1)}(n)$ .

We also define a free energy analog of Eq. B3 by

$$\Delta_1 G_T(n) = [G_T(1) + G_T^{\text{tot}}(n-1)] - G_T^{\text{tot}}(n), \quad (\text{B5})$$

One can define a particle isomeric free energy  $G_{\text{Iso}}$  by the same strategy as used for Eq. 19. In particular we define  $G_{\text{Iso}}$  as the excess free energy because there is more than one isomer:

$$G_{\text{Iso}} = G - G^{(\gamma=1)} \quad (\text{B6})$$

where  $G^{(\gamma)}$  is the free energy of isomer  $\gamma$ . By the definition of free energy, we have

$$e^{-G/RT} = \sum_{\gamma} e^{-G^{(\gamma)}/RT} \quad (\text{B7})$$

With this notation we can write Eq. 5 as

$$P_{\gamma} = \frac{e^{-G^{(\gamma)}/RT}}{\sum_{\gamma} e^{-G^{(\gamma)}/RT}} \quad (\text{B8})$$

Combining (B6) and (B7) with (B8) for  $\gamma = 1$  yields:

$$G_{\text{Iso}} = kT \ln P_1 \quad (\text{B9})$$

where  $P_1$  is the nonseparable probability of the global minimum given by Eq. 5.

### Additional discussion

Although we have used the second finite difference to discuss particle stability in Section 4, one can also use the first finite difference. The first finite difference of the total energy ( $\Delta_1 E_e^{(1)}(n)$ ) is the energy needed to remove one Al atom from the cluster or nanoparticle and is defined by Baletto and Ferrando<sup>5</sup> as

$$\Delta_1 E_e^{(1)}(n) = [E_e(1) + E_e^{(1)}(n-1)] - E_e^{(1)}(n), \quad (C1)$$

First differences of  $E_T^{\text{tot}}(n)$  and  $G_T^{\text{tot}}(n)$  are defined analogously. First finite differences are shown in Figs. S3 and S4. Analysis of the first finite differences led to similar conclusions as analysis of the second finite differences, in particular prominent peaks on the  $\Delta_1 E_e^{(1)}(n)$  plot are found at  $n = 13, 19, 23, 26, 32, 38$  and  $61$ . The peak appearing in Fig. 9 at  $n = 55$  is buried in the plateau encompassing  $n = 52 - 55$  in Fig. S3(a). It seems that another peak is building up in Fig. S3(a) after  $n = 65$ . The high peaks in Fig. S2(a) appear at  $n = 13, 19, 23, 38, 55$  and  $61$ , and therefore these numbers are candidates for the magic numbers of  $\text{Al}_n$  particles based on global minima.

In Fig. S7, 3D plots of  $P_\gamma$  vs. temperature and energy of the isomers ( $\Delta E$ , which is potential energy relative to the global minimum, is called  $DE$  in the figures) are depicted for several particles with  $n = 13$  (Fig. S7(a)),  $19$  (Fig. S7(b)),  $23$  (Fig. S7(c)),  $38$  (Fig. S7(d)),  $55$  (Fig. S7(e)), and  $61$  (Fig. S7(f)). The selected particles are the five candidates for the magic particles plus  $\text{Al}_{61}$ , for which the third lowest-energy isomer is the dominant structure even at room temperature. In Fig. S7, a red line perpendicular to the  $\Delta E$  axis corresponds to an isomer at that energy. For  $n = 13, 19, 23$ , and  $55$ , the global minimum always has the largest probability, while other higher-energy isomers always have very small probabilities. For  $n = 38$ , the probability of the global minimum begins to drop after 300 K, and after 600 K it becomes very small. The probabilities of the fourth- and sixth-lowest energy isomer of  $\text{Al}_{38}$  are non-negligible even at 400 K. For  $n = 61$ , it is interesting that the probability of the global minimum is negligible over the whole temperature range. Although the probability of the third lowest-energy isomer is high at room temperature (see also Fig. 9(a) (top)), it drops quickly as temperature increases. At 500 K, it drops to just about 23%. This may be because that isomer has more low-frequency vibrational modes than the global minimum.

Plots of  $D$  (defined by Eq. 11) vs. temperature  $T$  and equilibrium isomer energy  $\Delta E$  are given in Figs. 11 and S8.

For  $\text{Al}_{13}$ , the second isomer is higher in energy by 1.01 eV. As a result, up to 1000 K, Fig. S8(a) shows that the probability of the global minimum is almost 100%. It begins to drop after 1000 K, and it drops quickly after 1200 K, but it is still more than 60% at 1500 K. After 1000 K, the probabilities of isomers at about 1.0 eV and 1.2 eV begin to increase. Therefore, we would expect  $\text{Al}_{13}$  to have a melting point around 1200 K.

For  $\text{Al}_{19}$  and  $\text{Al}_{23}$ , Fig. S8 shows that the probability of the global minimum drops quickly after 1000 K and 800 K, respectively. For  $\text{Al}_{19}$ , two peaks appear after 800 K at around 0.6 eV and 1.0 eV, and the second peak is higher than the first peak at about 1500 K. For  $\text{Al}_{23}$ , there are three peaks after 800 K, at about 0.6 eV, 0.8 eV, and 0.9 eV, respectively.

For  $\text{Al}_{38}$ , Fig. 11 shows that the global minimum dominates only up to 400 K. Afterwards, the isomers at about 0.6 eV begin to make non-negligible contribution and after about 1000 K, their contribution begins to decrease, and isomers between 0.7 – 0.9 eV begin to make larger contributions. Therefore, we would expect that  $\text{Al}_{38}$  may have a much smaller melting point, and it may be difficult to make an  $\text{Al}_{38}$  particle with a well ordered structure, i.e. the global minimum. Therefore, for an experimental observables point of view  $n = 38$  should not be classified as a magic number for  $\text{Al}_n$  particles.

For  $\text{Al}_{55}$ , the probability of the global minimum begins to drop at about 500 K. Then the probability of the isomers between 0.70 – 0.75 eV begins to rise quickly, and reaches a maxim at about 700 K. After 700 K, the probability between 0.70 – 0.75 eV drops slowly but is still higher than 80% even at 1500 K. Fig. S8(d) shows that the probability of each  $\text{Al}_{55}$  isomer in this energy range is very small. However, the MDSQ method located 205 isomers in this energy range. Therefore, even if individual isomers make small contributions, together they make a major contribution to the properties of the  $\text{Al}_{55}$  droplet, since  $\text{Al}_{55}$  melts at about 600 K.<sup>37</sup> Therefore, unlike  $\text{Al}_{19}$ ,  $\text{Al}_{23}$ , and  $\text{Al}_{38}$ , where the liquid state is composed of structures in a much wider energy range, the melting of  $\text{Al}_{55}$  is some respects like a transition between two energy levels.

We have checked the structures of some  $\text{Al}_{55}$  isomers between 0.70 – 0.75 eV. These structures can be obtained by removing one vertex atom on the  $C_5$  rotation axis of the global minimum (an icosahedron, see Fig. 4) and placing it on top of three aluminum atoms in one face of the icosahedral structure. This is the reason that these isomers fall in a narrow energy range.

For  $\text{Al}_{61}$ , even at low temperatures such as 400 K, the particle has a wide distribution of potential energies. Above 400 K,  $\text{Al}_{61}$  particle can be viewed as a mixture of isomers in an energy range between 0.4 and 0.8 eV (see Fig. S8(e)). It is therefore very hard to make an  $\text{Al}_{61}$  particle with a well defined structure.

The quantity  $\Delta_1 G_T^{\text{tot}}(n)$  is shown as a function of cluster size in Fig. S3(c) for 300 and 1500 K, and plots for at 500 and 800 K are given in Fig. S4(b). At 300 K,  $\Delta_1 G_T(n)$  shows trends very similar to those for  $\Delta_1 E_e^{(1)}(n)$  in Fig. S3(a) and for  $\Delta_1 E_T^{\text{tot}}$  in Fig. S3(b). The three plots agree well with each other for the locations of the peaks, i.e., for the potential magic numbers. They also predict that  $\text{Al}_{14}$  is one of the most unstable particles. There are also some subtle differences among the three properties, for example, the  $\Delta_1 G_T(n)$  plot shows a valley at  $n = 57$ , whereas the plots of  $\Delta_1 E_T^{\text{tot}}(n)$  and  $\Delta_1 E_e^{(1)}(n)$  show a valley at  $n = 56$ . However, as temperature increases, some peaks in the plots of  $\Delta_1 E_T^{\text{tot}}(n)$  become less prominent, and some others even vanish, for example, the peak at  $n = 38$  disappears at the other three temperatures. Some peaks shift, for example, the peak at  $n = 19$  below 1500 K shifts to  $n = 20$  at 1500 K, and the peak at  $n = 38$  at 300 K shifts to  $n = 39$  at higher temperatures. Valleys also shift, for example, on the  $\Delta_1 E_T^{\text{tot}}(n)$  plot, the valleys at  $n = 56$  at 300 and 500 K shift to  $n = 57$ , and the valley at  $n = 50$  at 300 and 500 K shifts to 49 at 800 K, whereas on the  $\Delta_1 G_T(n)$  plot it shifts to  $n = 49$  at 500 K. In general, the peaks and valleys on the  $\Delta_1 E_T^{\text{tot}}(n)$  and  $\Delta_1 E_e^{(1)}(n)$  plots are more prominent than those on the  $\Delta_1 G_T(n)$  plot.

Except for a few subtle differences at  $n = 34$  and 35,  $n = 48$  and 49, and  $n = 56 - 58$ ,  $\Delta_2 E_T^{\text{tot}}(n)$  has almost the same trends as  $\Delta_2 G_T^{\text{tot}}(n)$ . It is interesting that the high peak at  $n = 55$  on the  $\Delta_2 G_T(n)$  plot vanishes and shifts to  $n = 56$  at 500 K, while on the  $\Delta_2 E_T^{\text{tot}}(n)$  plot the same happens at 800 K. Furthermore the peak at  $n = 56$  does not vanish at 1500 K, as it does on the  $\Delta_2 G_T(n)$  plot.

The first ( $\Delta_1 G_T(n)$ ) and second ( $\Delta_2 G_T(n)$ ) differences in free energy are better quantities for characterizing the stability of particles than are other quantities without entropy contributions ( $\Delta_1 E_T(n)$  and  $\Delta_2 E_T(n)$ ) or even without any thermal or ZPE contributions ( $\Delta_1 E_e^{(1)}(n)$  and  $\Delta_2 E_e^{(1)}(n)$ ). A key point, though, as also mentioned in Sect. 5, is that the  $\Delta_2 E_T(n)$  and  $\Delta_2 G_T(n)$  plots are more similar than different; this shows the importance of thermal energy and ZPE effects relative to entropic effects.

Table S1. Cohesive energies (CE, eV/atom) of the lowest-energy minima located. These values are plotted in Fig. 6, and those with  $n \geq 12$  are also plotted in Fig. S1.

Cluster size	CE	Cluster size	CE	Cluster size	CE	Cluster size	CE
2	0.971	18	2.520	34	2.703	50	2.793
3	1.399	19	2.563	35	2.709	51	2.797
4	1.705	20	2.568	36	2.715	52	2.805
5	1.867	21	2.574	37	2.722	53	2.813
6	2.024	22	2.587	38	2.740	54	2.820
7	2.103	23	2.615	39	2.739	55	2.827
8	2.165	24	2.617	40	2.741	56	2.822
9	2.215	25	2.626	41	2.748	57	2.821
10	2.269	26	2.645	42	2.749	58	2.824
11	2.311	27	2.649	43	2.755	59	2.828
12	2.374	28	2.661	44	2.761	60	2.829
13	2.454	29	2.667	45	2.764	61	2.837
14	2.446	30	2.670	46	2.772	62	2.836
15	2.473	31	2.676	47	2.776	63	2.838
16	2.484	32	2.690	48	2.783	64	2.841
17	2.497	33	2.694	49	2.788	65	2.846

Table S2. The probability (as a percentage) of finding the four lowest-energy minima at 300 K used in Figs. S2A–S2D with “1st” representing the global minimum, “2nd” the second lowest-energy isomer, and so on.

	1st	2nd	3rd	4th	1st	2nd	3rd	4th
<i>n</i>	IC	IC	IC	IC	IS	IS	IS	IS
2	100.0	NA	NA	NA	100.0	NA	NA	NA
3	100.0	NA	NA	NA	100.0	NA	NA	NA
4	100.0	NA	NA	NA	100.0	NA	NA	NA
5	99.8	0.2	0.00	0.00	99.9	0.07	0.00	0.00
6	100.0	0.00	NA	NA	100.0	0.00	NA	NA
7	99.4	0.5	0.04	0.00	99.9	0.14	0.00	0.00
8	99.7	0.2	0.08	0.00	99.9	0.04	0.02	0.00
9	39.3	60.4	0.3	0.01	50.5	49.3	0.2	0.00
10	100.0	0.01	0.00	0.01	99.9	0.09	0.01	0.00
11	98.9	0.01	0.02	0.02	99.7	0.01	0.01	0.01
12	100.0	0.00	0.00	0.00	100.0	0.00	0.00	0.00
13	100.0	0.00	0.00	0.00	100.0	0.00	0.00	0.00
14	74.6	17.3	4.7	1.7	70.8	21.3	5.3	1.3
15	90.7	9.2	0.06	0.00	97.3	2.7	0.03	0.00
16	80.9	10.2	7.9	0.8	58.3	20.3	18.9	1.9
17	24.2	2.2	0.9	1.6	6.8	3.4	2.7	1.6
18	90.3	9.6	0.01	0.01	68.6	31.3	0.01	0.01
19	100.0	0.00	0.00	0.00	100.0	0.00	0.00	0.00
20	98.5	0.14	0.3	0.3	98.0	0.45	0.45	0.45
21	70.9	10.1	9.9	6.3	67.7	14.1	8.9	6.3
22	20.1	47.5	25.9	0.9	55.3	25.9	15.5	0.4
23	100.0	0.00	0.00	0.00	100.0	0.00	0.00	0.00

24	73.2	13.2	13.4	0.04	73.1	14.1	12.7	0.04
25	74.5	5.4	11.7	3.12	78.3	13.4	4.7	1.6
26	100.0	0.00	0.00	0.00	100.0	0.00	0.00	0.00
27	99.1	0.8	0.01	0.01	99.7	0.3	0.00	0.00
28	99.9	0.04	0.01	0.01	100.0	0.01	0.01	0.01
29	65.8	33.3	0.5	0.06	93.8	5.4	0.5	0.07
30	76.8	2.15	1.5	0.6	48.8	3.7	2.9	2.9
31	2.3	17.4	7.3	7.35	19.4	16.1	7.9	7.9
32	10.6	88.8	0.06	0.11	81.2	17.5	0.2	0.12
33	27.0	2.15	2.15	2.15	30.1	6.3	6.3	6.3
34	43.2	1.3	0.35	15.2	95.8	1.3	0.5	0.4
35	96.8	0.8	0.5	1.2	78.7	7.2	5.5	4.3
36	25.8	10.7	0.00	5.1	25.3	11.5	6.7	6.1
37	3.8	0.11	14.4	1.4	42.5	34.7	3.6	2.5
38	99.7	0.1	0.01	0.00	100.0	0.00	0.00	0.00
39	0.1	44.4	28.0	12.8	52.3	25.6	21.8	0.09
40	98.2	0.6	0.09	0.09	52.2	30.0	3.6	3.6
41	8.85	0.2	0.2	0.2	7.02	3.0	3.0	3.0
42	2.4	1.6	1.6	1.6	24.7	9.55	9.55	9.55
43	0.00	21.5	21.5	5.5	35.1	16.2	16.2	5.2
44	97.6	0.00	0.4	0.4	93.7	1.4	0.6	0.5
45	24.9	24.9	25.0	0.4	12.5	12.5	12.5	6.85
46	72.9	1.2	0.4	3.3	37.9	33.7	13.3	1.65
47	48.9	11.3	4.2	4.25	31.7	20.3	5.3	5.3
48	100.0	0.00	0.00	0.00	99.9	0.04	0.03	0.01
49	87.2	11.2	1.35	0.07	90.9	9.1	0.02	0.00
50	1.6	8.9	7.4	6.4	100.0	0.01	0.00	0.00

51	23.6	13.3	12.0	11.6	23.8	12.7	11.9	11.7
52	38.4	21.8	19.7	12.5	40.1	21.5	20.0	11.7
53	40.0	37.00	23.0	0.00	40.4	37.5	22.1	0.00
54	100.0	0.00	0.00	0.00	100.0	0.00	0.00	0.00
55	100.0	0.00	0.00	0.00	100.0	0.00	0.00	0.00
56	0.09	0.2	0.13	1.7	3.9	3.7	3.2	2.2
57	58.7	2.8	2.8	3.8	90.1	0.75	0.75	0.75
58	8.8	3.3	2.7	2.7	87.3	1.45	0.8	0.8
59	66.7	9.3	12.6	1.6	68.3	16.9	14.3	0.12
60	85.6	0.5	5.8	1.85	73.4	14.7	10.3	0.2
61	0.08	0.00	95.3	0.85	100.0	0.01	0.00	0.00
62	86.1	7.3	0.00	0.00	87.5	11.8	0.2	0.08
63	0.00	0.00	3.1	0.00	74.2	10.9	4.9	3.11
64	0.00	0.00	0.00	0.00	95.5	3.3	0.3	0.14
65	0.01	0.01	0.00	0.00	48.5	48.5	3.0	0.05

---

Table S3. The probability (as a percentage) of finding the four lowest-energy minima at 1500 K used in Figs. S2A–S2D with “1st” representing the global minimum, “2nd” the second lowest-energy isomer, and so on.

	1st	2nd	3rd	4th	1st	2nd	3rd	4th
<i>n</i>	IC	IC	IC	IC	IS	IS	IS	IS
2	100.0	NA	NA	NA	100.0	NA	NA	NA
3	100.0	NA	NA	NA	100.0	NA	NA	NA
4	100.0	NA	NA	NA	100.0	NA	NA	NA
5	54.3	33.8	11.7	0.12	78.8	18.7	2.5	0.02
6	89.0	11.0	NA	NA	99.8	0.2	NA	NA
7	15.0	15.7	19.3	1.9	60.3	16.1	7.8	2.1
8	27.6	30.1	26.4	1.35	66.5	13.7	11.5	3.4
9	21.4	33.9	13.8	7.05	31.7	31.5	10.7	4.6
10	35.0	1.0	2.5	5.85	35.6	8.7	5.7	4.9
11	2.8	0.5	1.25	1.25	8.8	1.3	1.2	1.2
12	46.2	3.7	6.8	0.6	89.4	0.9	0.6	0.5
13	62.6	4.2	4.1	2.6	99.6	0.04	0.04	0.03
14	29.5	18.4	15.3	17.0	30.0	23.6	17.9	13.5
15	17.1	30.8	7.7	5.6	31.9	15.5	6.2	3.5
16	33.4	10.1	8.0	5.0	15.0	12.2	12.0	7.6
17	6.1	1.0	0.5	1.3	1.5	1.3	1.3	1.1
18	7.4	1.5	1.0	1.9	8.0	6.8	1.3	1.2
19	27.2	3.5	3.8	3.2	90.4	0.5	0.5	0.5
20	13.1	1.45	2.9	2.9	18.1	6.2	6.2	6.2
21	10.2	5.0	7.2	5.9	9.85	7.2	6.6	6.12
22	0.8	3.3	2.75	1.8	3.8	3.3	3.0	1.4

23	8.05	1.85	0.8	0.04	52.0	0.8	0.6	0.6
24	8.1	5.45	6.1	1.9	12.0	8.6	8.45	2.6
25	3.03	0.9	4.3	2.75	6.5	4.55	3.7	3.0
26	25.6	4.9	0.9	1.1	20.3	2.0	1.4	1.4
27	3.8	3.7	2.0	2.0	7.9	2.4	0.95	0.95
28	6.5	2.9	0.6	1.2	11.5	1.9	1.8	1.8
29	2.0	9.7	1.2	0.6	4.9	2.8	1.7	1.15
30	4.0	0.9	0.8	0.3	1.2	0.7	0.7	0.7
31	0.2	1.3	1.0	1.0	0.8	0.8	0.7	0.7
32	0.6	13.6	0.3	1.0	3.0	2.2	0.9	0.8
33	0.9	0.25	0.25	0.25	1.2	0.9	0.9	0.9
34	0.04	0.04	0.02	1.1	1.6	0.7	0.6	0.5
35	6.1	0.4	0.3	0.8	1.3	0.8	0.8	0.7
36	0.6	0.5	0.00	0.4	0.5	0.4	0.4	0.4
37	0.01	0.00	0.3	0.05	0.8	0.8	0.5	0.5
38	0.00	0.15	0.04	0.03	20.4	0.6	0.4	0.4
39	0.00	0.1	0.08	2.2	3.0	2.6	2.5	0.8
40	8.4	0.1	0.08	0.08	1.25	1.1	0.7	0.7
41	0.00	0.00	0.00	0.00	1.2	1.0	1.0	1.0
42	0.03	0.04	0.04	0.04	0.5	0.4	0.4	0.4
43	0.00	0.5	0.5	0.3	0.6	0.5	0.5	0.4
44	1.85	0.00	0.5	0.4	0.9	0.4	0.3	0.3
45	1.5	1.5	1.5	0.04	0.5	0.5	0.5	0.4
46	2.2	0.04	0.03	1.2	1.2	1.2	1.0	0.65
47	1.1	0.4	0.4	0.4	0.85	0.8	0.6	0.6
48	8.9	0.00	0.03	0.02	3.7	0.8	0.7	0.6

49	0.07	0.06	0.9	0.4	4.3	2.7	0.8	0.5
50	0.00	0.02	0.05	0.05	5.7	0.8	0.6	0.6
51	0.12	0.11	0.11	0.1	3.65	3.2	3.2	3.2
52	0.3	0.3	0.3	0.3	14.4	12.7	12.6	11.3
53	0.35	0.3	0.3	0.01	21.9	21.5	19.4	0.8
54	0.10	0.7	0.02	0.02	49.6	0.2	0.2	0.2
55	0.01	0.03	0.02	0.01	58.8	0.3	0.25	0.25
56	0.04	0.07	0.07	1.1	2.25	2.2	2.2	2.0
57	0.11	0.2	0.2	0.3	3.4	1.3	1.3	1.3
58	0.00	0.01	0.01	0.01	1.9	0.8	0.8	0.8
59	0.03	0.01	0.02	0.09	3.4	2.5	2.5	0.95
60	0.2	0.00	0.06	0.4	1.2	0.9	0.8	0.4
61	0.00	0.00	0.08	0.00	11.1	1.6	1.5	1.0
62	0.04	0.02	0.00	0.00	1.9	1.3	0.6	0.5
63	0.00	0.00	0.01	0.00	1.15	0.8	0.7	0.6
64	0.00	0.00	0.00	0.00	1.5	0.8	0.5	0.4
65	0.00	0.00	0.00	0.00	4.5	4.5	2.6	1.15

---

Table S4. The cumulative probability (as a percentage) of the  $N$  lowest-energy isomers as a function of cluster size at 300 K.

$n \backslash N$	1	2	4	8	16	32	64
2	100.0	NA	NA	NA	NA	NA	NA
3	100.0	NA	NA	NA	NA	NA	NA
4	100.0	NA	NA	NA	NA	NA	NA
5	99.8	100.0	100.0	NA	NA	NA	NA
6	100.0	100.0	NA	NA	NA	NA	NA
7	99.4	99.96	100.0	100.0	NA	NA	NA
8	99.7	99.92	100.0	100.0	NA	NA	NA
9	39.3	99.7	99.99	100.0	100.0	NA	NA
10	99.96	99.97	99.98	99.99	100.0	NA	NA
11	98.9	98.9	99.0	99.0	99.2	99.6	100.0
12	100.0	100.0	100.0	100.0	100.0	100.0	100.0
13	100.0	100.0	100.0	100.0	100.0	100.0	100.0
14	74.6	91.9	98.3	100.0	100.0	100.0	100.0
15	90.7	99.93	99.99	100.0	100.0	100.0	100.0
16	80.85	91.0	99.7	99.99	100.0	100.0	100.0
17	24.2	26.3	28.8	32.9	41.1	57.5	91.1
18	90.3	99.95	99.97	99.98	99.99	99.99	100.0
19	100.0	100.0	100.0	100.0	100.0	100.0	100.0
20	98.5	98.7	99.2	99.6	99.96	100.0	100.0
21	70.9	81.0	97.25	99.8	99.99	100.0	100.0
22	20.1	67.7	94.5	98.3	99.1	99.6	99.8
23	100.0	100.0	100.0	100.0	100.0	100.0	100.0
24	73.25	86.45	99.92	100.0	100.0	100.0	100.0
25	74.5	79.9	94.7	99.3	99.6	99.97	100.0

26	100.0	100.0	100.0	100.0	100.0	100.0	100.0
27	99.1	99.94	99.96	100.0	100.0	100.0	100.0
28	99.9	99.94	99.95	100.0	100.0	100.0	100.0
29	65.8	99.15	99.7	99.87	99.97	99.98	99.99
30	76.8	79.0	81.0	88.3	94.2	98.5	99.6
31	2.3	19.7	34.4	50.1	72.3	98.4	99.7
32	10.6	99.4	99.5	99.6	99.8	99.9	100.0
33	26.95	29.1	33.4	39.2	58.3	98.1	99.7
34	43.2	44.5	60.05	71.3	80.7	93.1	98.1
35	96.8	97.6	99.3	99.7	99.8	99.9	99.96
36	25.8	36.5	41.6	46.1	49.3	67.55	90.2
37	3.77	3.9	19.7	29.4	70.7	90.8	96.0
38	99.7	99.8	99.8	99.90	99.97	99.98	99.99
39	0.11	44.5	85.4	93.4	93.9	96.4	99.91
40	98.2	98.8	99.0	99.15	99.94	99.97	99.98
41	8.85	9.1	9.6	10.4	12.3	16.0	96.2
42	2.4	4.0	7.1	36.8	41.7	45.5	89.95
43	0.00	21.5	48.5	77.95	92.3	95.0	97.4
44	97.6	97.6	98.4	98.8	99.0	99.5	99.7
45	24.9	49.85	75.2	78.8	91.5	95.0	98.65
46	72.9	74.1	77.8	91.2	99.4	99.7	99.94
47	48.9	60.1	68.6	85.6	94.0	97.0	97.7
48	100.0	100.0	100.0	100.0	100.0	100.0	100.0
49	87.2	98.4	99.8	99.93	99.95	99.98	99.99
50	1.6	10.4	24.3	35.2	77.5	87.55	94.6
51	23.6	36.9	60.5	92.4	99.97	100.0	100.0
52	38.4	60.2	92.4	100.0	100.0	100.0	100.0

53	40.0	77.0	100.0	100.0	100.0	100.0	100.0
54	100.0	100.0	100.0	100.0	100.0	100.0	100.0
55	100.0	100.0	100.0	100.0	100.0	100.0	100.0
56	0.09	0.25	2.1	8.9	28.55	66.3	100.0
57	58.7	61.4	68.0	83.0	97.6	99.89	99.97
58	8.8	12.2	17.55	24.8	40.1	74.8	96.8
59	66.7	75.9	90.1	97.8	99.5	99.8	99.90
60	85.55	86.05	93.7	96.0	96.3	97.7	98.9
61	0.08	0.08	96.2	96.4	96.6	98.3	99.0
62	86.1	93.5	93.5	95.7	96.8	98.2	99.5
63	0.00	0.00	3.1	79.85	80.6	87.9	96.0
64	0.00	0.00	0.01	0.9	13.0	49.3	73.6
65	0.01	0.03	0.03	28.6	53.0	60.5	85.7

---

Table S5. The cumulative probability (as a percentage) of the  $N$  lowest-energy isomers as a function of cluster size at 1500 K.

$nN$	1	2	4	8	16	32	64
2	100.0	NA	NA	NA	NA	NA	NA
3	100.0	NA	NA	NA	NA	NA	NA
4	100.0	NA	NA	NA	NA	NA	NA
5	54.3	88.15	100.0	NA	NA	NA	NA
6	89.0	100.0	NA	NA	NA	NA	NA
7	15.0	30.6	51.9	75.5	NA	NA	NA
8	27.6	57.7	85.4	98.4	NA	NA	NA
9	21.35	55.2	76.1	86.55	99.8	NA	NA
10	35.0	36.0	44.4	60.7	87.9	NA	NA
11	2.8	3.3	5.8	10.85	21.2	52.1	90.75
12	46.2	49.9	57.35	65.0	77.2	89.5	97.35
13	62.6	66.9	73.6	83.9	88.45	95.35	98.4
14	29.5	47.85	80.2	98.1	99.2	99.6	99.85
15	17.1	47.9	61.1	71.9	75.0	80.7	98.6
16	33.4	43.5	56.55	70.9	80.5	94.9	99.5
17	6.1	7.1	9.0	13.3	21.85	39.1	74.4
18	7.4	8.8	11.7	15.5	21.6	35.4	51.95
19	27.2	30.7	37.6	40.7	46.0	53.2	64.0
20	13.1	14.6	20.4	35.35	75.0	93.3	96.3
21	10.2	15.2	28.3	41.1	53.5	66.6	83.2
22	0.8	4.12	8.7	15.9	21.6	33.0	51.8
23	8.05	9.9	10.8	18.2	24.1	30.7	38.9
24	8.1	13.5	21.5	33.6	42.3	52.2	58.5
25	3.03	3.9	10.9	23.0	28.0	39.25	59.5

26	25.6	30.5	32.4	35.2	40.5	46.6	52.6
27	3.8	7.5	11.5	19.0	27.1	34.0	40.6
28	6.5	9.4	11.2	22.9	27.4	34.75	43.8
29	2.0	11.7	13.5	16.1	21.45	25.1	33.2
30	4.0	4.95	6.0	9.7	13.9	21.4	29.7
31	0.2	1.4	3.4	7.8	17.6	31.0	38.3
32	0.6	14.2	15.5	16.8	22.9	29.5	36.5
33	0.9	1.1	1.6	2.7	7.9	26.3	33.0
34	0.04	0.09	1.2	3.2	6.4	14.0	21.1
35	6.1	6.5	7.7	9.4	11.75	16.1	22.9
36	0.6	1.1	1.5	1.9	3.6	15.7	32.1
37	0.01	0.02	0.4	0.9	4.9	9.97	15.1
38	0.00	0.14	0.2	1.9	6.4	7.9	10.4
39	0.00	0.1	2.4	4.0	5.7	15.3	33.4
40	8.4	8.5	8.6	8.8	13.8	16.3	22.2
41	0.00	0.00	0.00	0.00	0.00	0.00	8.9
42	0.03	0.07	0.2	1.1	2.3	3.75	27.4
43	0.00	0.5	1.3	3.9	6.6	9.3	17.1
44	1.85	1.85	2.75	3.4	4.5	9.2	13.4
45	1.5	2.9	4.4	4.95	8.6	11.5	17.6
46	2.2	2.3	3.5	8.4	12.6	15.6	24.1
47	1.1	1.5	2.4	4.05	7.0	9.9	14.2
48	8.9	8.9	8.95	9.0	10.4	11.3	16.1
49	0.07	0.13	1.4	3.4	5.0	7.95	12.1
50	0.00	0.02	0.11	0.2	1.4	2.8	5.3
51	0.12	0.2	0.4	0.8	1.15	8.55	12.4
52	0.3	0.6	1.2	1.6	2.6	7.3	13.7

53	0.35	0.7	1.0	1.5	3.1	5.5	9.0
54	0.1	0.8	0.8	0.8	1.0	6.9	8.6
55	0.01	0.04	0.07	0.2	2.35	9.8	28.8
56	0.04	0.11	1.3	5.9	18.9	44.05	67.3
57	0.11	0.3	0.8	2.0	3.5	5.4	7.4
58	0.00	0.01	0.04	0.08	0.2	1.3	4.9
59	0.03	0.04	0.15	1.0	2.8	5.8	7.6
60	0.2	0.2	0.6	1.05	1.2	3.7	9.1
61	0.00	0.00	0.08	0.13	0.2	1.5	4.8
62	0.04	0.06	0.06	0.8	1.7	4.2	8.5
63	0.00	0.00	0.01	0.8	0.8	2.3	7.6
64	0.00	0.00	0.00	0.00	0.13	1.4	3.7
65	0.00	0.00	0.00	0.03	0.07	0.11	6.9

---

Figure captions:

- Figure S1. Cohesive energies of the lowest-energy minima as a function of  $n^{-1/3}$  with  $n = 12 - 65$ , where  $n$  is the number of atoms in the aluminum particle.
- Figure S2(a). The probability of the global minimum at 300 K and 1500 K: (top) IC; (bottom) IS.
- Figure S2(b). The probability of the second-lowest-energy minimum at 300 K and 1500 K: (top) IC; (bottom) IS.
- Figure S2(c). The probability of the third-lowest-energy minimum at 300 K and 1500 K: (top) IC; (bottom) IS.
- Figure S2(d). The probability of the fourth-lowest-energy minimum at 300 K and 1500 K: (top) IC; (bottom) IS.
- Figure S3. First energy differences as a function of cluster size: (a)  $\Delta_1 E_e^{(1)}(n)$ , which is independent of temperature, (b)  $\Delta_1 E_T^{\text{tot}}(n)$  at 300 and 1500 K, (b)  $\Delta_1 G_T(n)$  at 300 and 1500 K. Note:  $\Delta G_T$  is labeled  $\Delta G_T$  in figures.
- Figure S4. First energy differences functions of cluster size at 500 and 800 K: (a)  $\Delta_1 E_T^{\text{tot}}(n)$  and (b)  $\Delta_1 G_T^{\text{t}}(n)$ . Note:  $\Delta G_T$  is labeled  $\Delta G_T^{\text{tot}}$  in figures.
- Figure S5. Second energy difference,  $\Delta_2 E_T^{\text{tot}}(n)$ , as a function of cluster size at 300 and 1500 K.
- Figure S6. Second energy differences as a function of cluster size at 500 and 800 K: (a)  $\Delta_2 E_T^{\text{tot}}(n)$ ; (b)  $\Delta_2 G_T(n)$ . Note:  $\Delta G_T$  is labeled  $\Delta G_T^{\text{tot}}$  in figures.
- Figure S7. 3D plots of  $P_\gamma$  vs.  $T$  (temperature in K) and  $DE$  (potential energy relative to the global minimum in eV) for particles with  $n = 13$  (a), 19 (b), 23 (c), 38 (d), 55 (e), and 61 (f).
- Figure S8. 3D plots of  $D$  (calculated by Eq. 10 with  $\delta E = 0.05$  eV) vs.  $T$  (temperature in K) and  $\Delta E$  (potential energy relative to the global minimum in eV, labeled  $DE$  in the figure) for  $n = 13$  (a), 19 (b), 23 (c), 55 (d), and 61 (e).

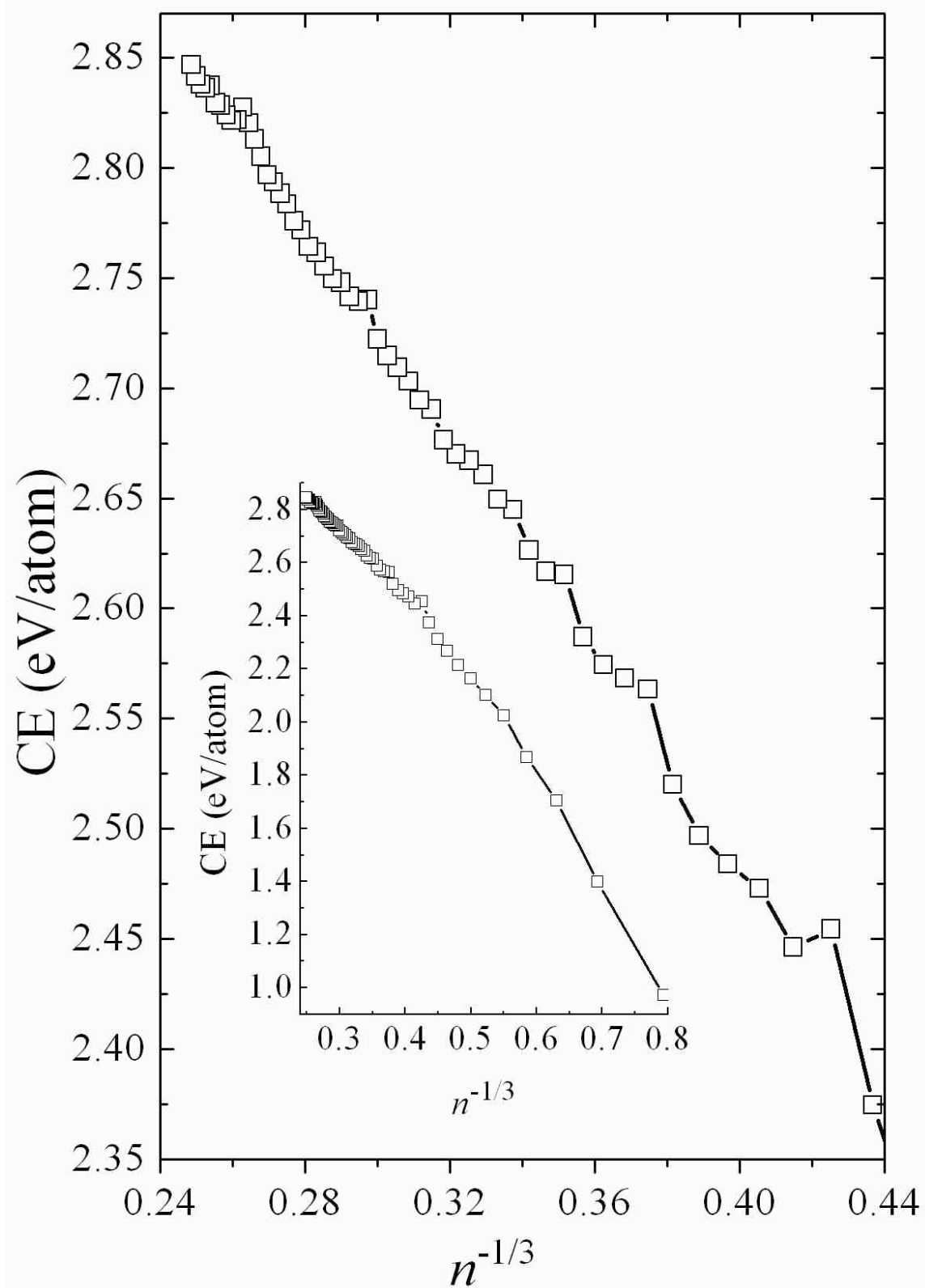


Fig. S1

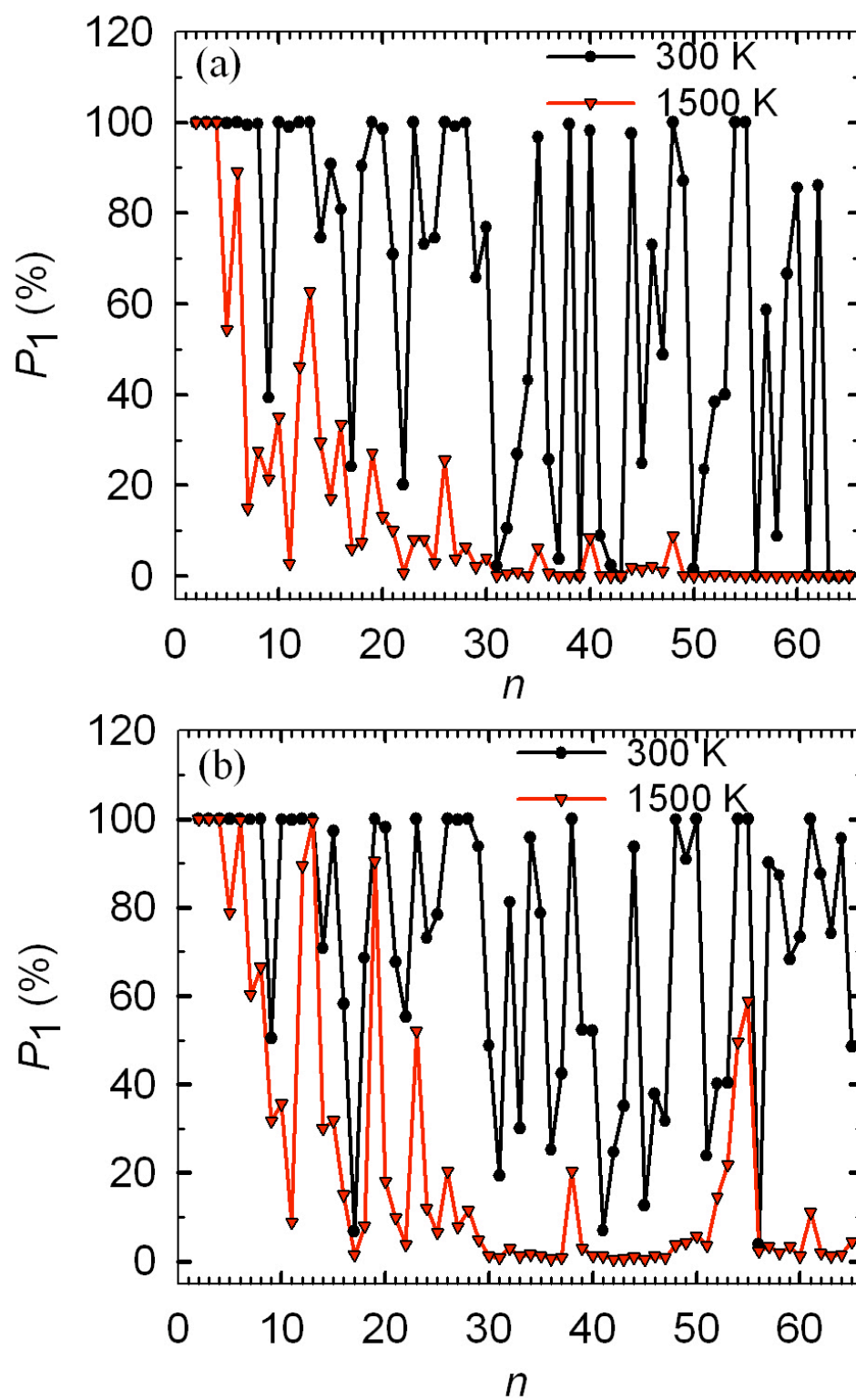


Fig. S2(a)

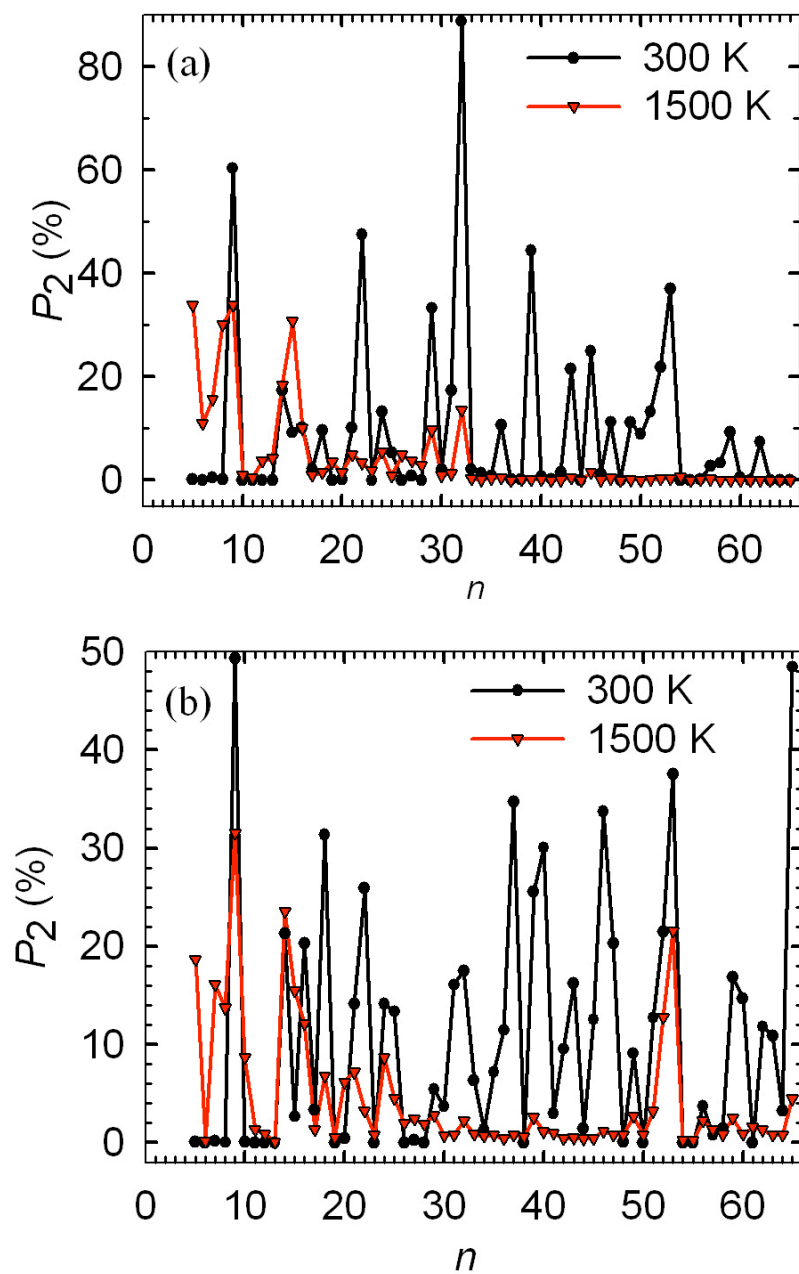


Fig. S2(b)

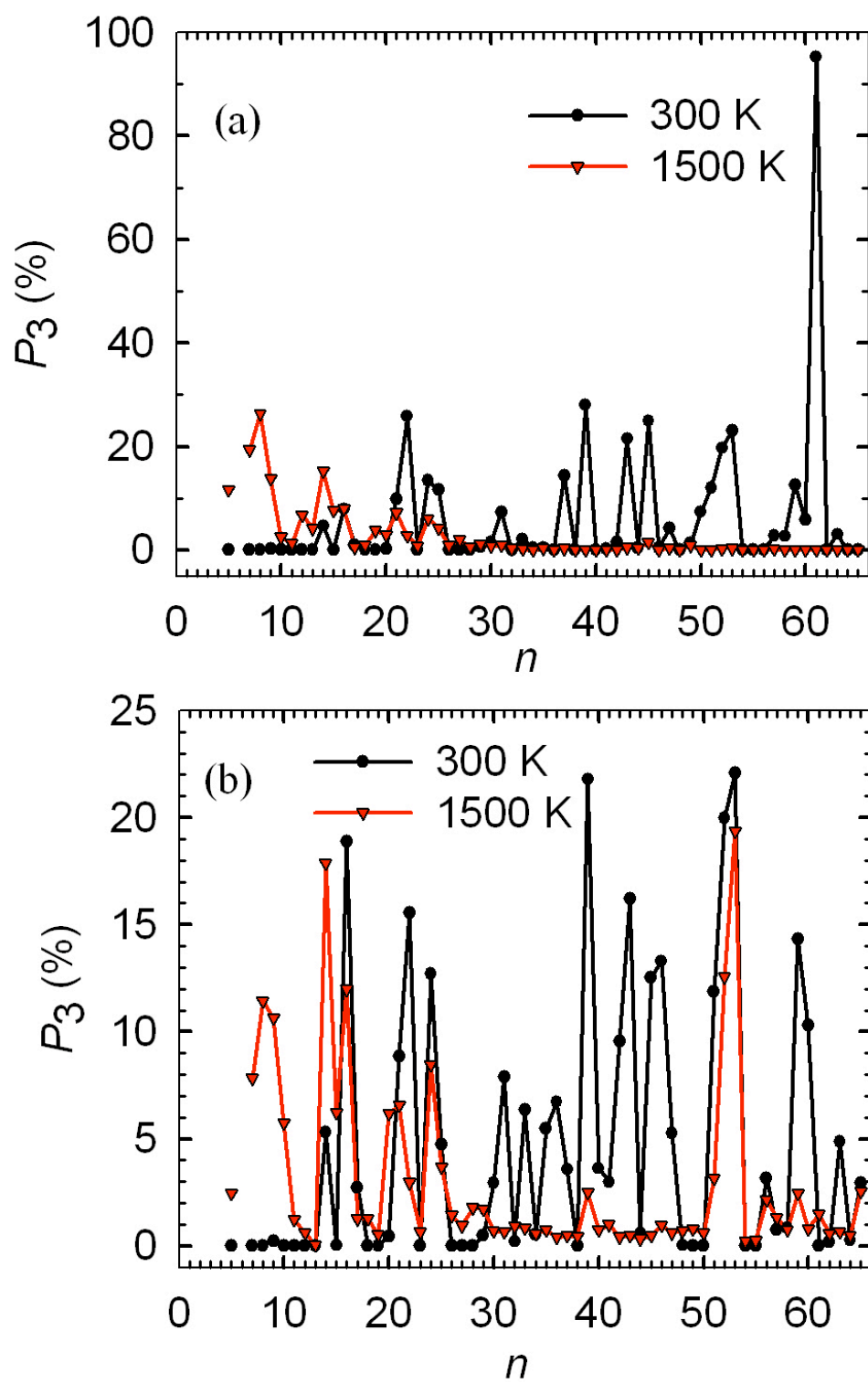


Fig. S2(c)

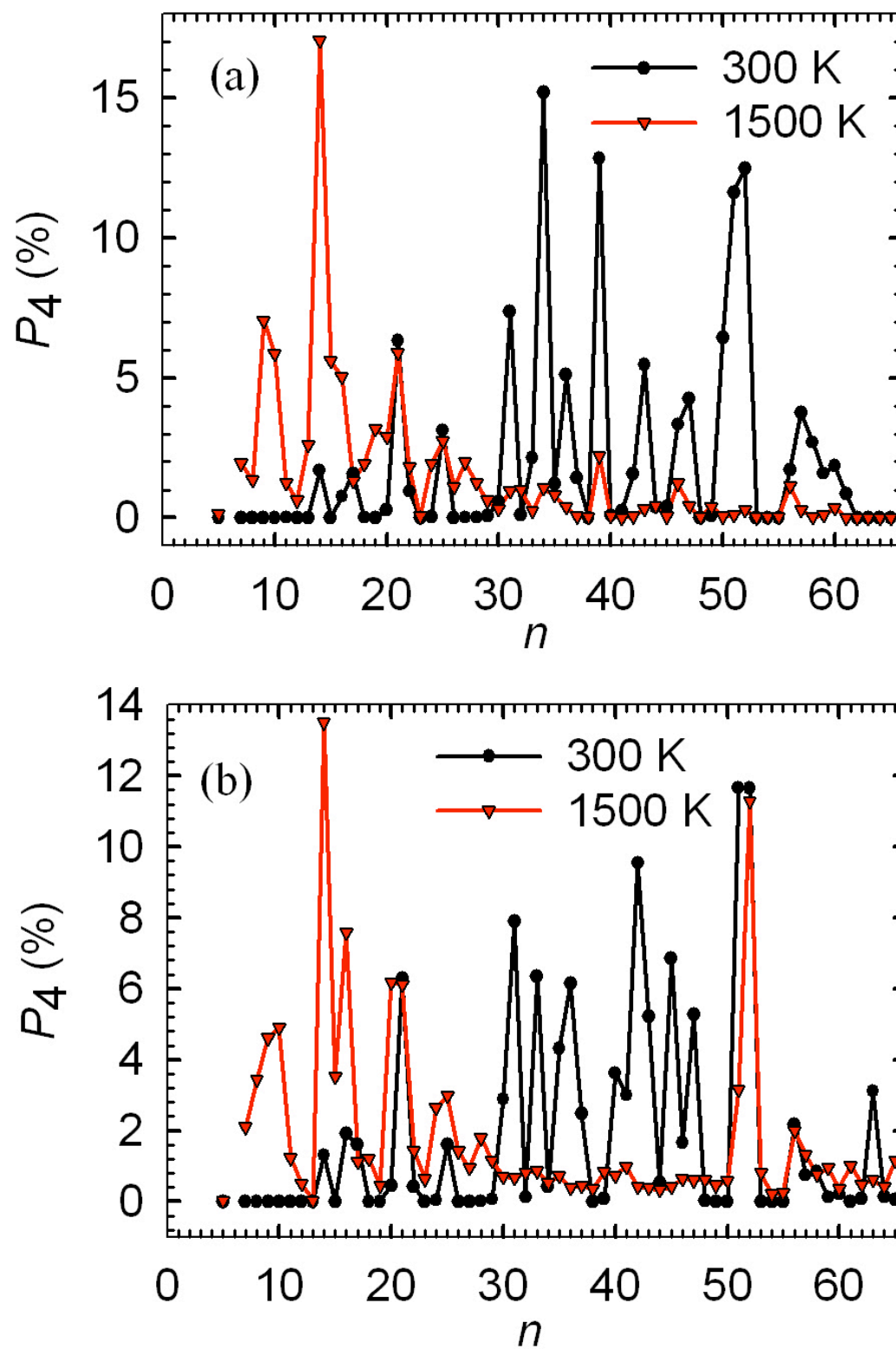


Fig. S2(d)

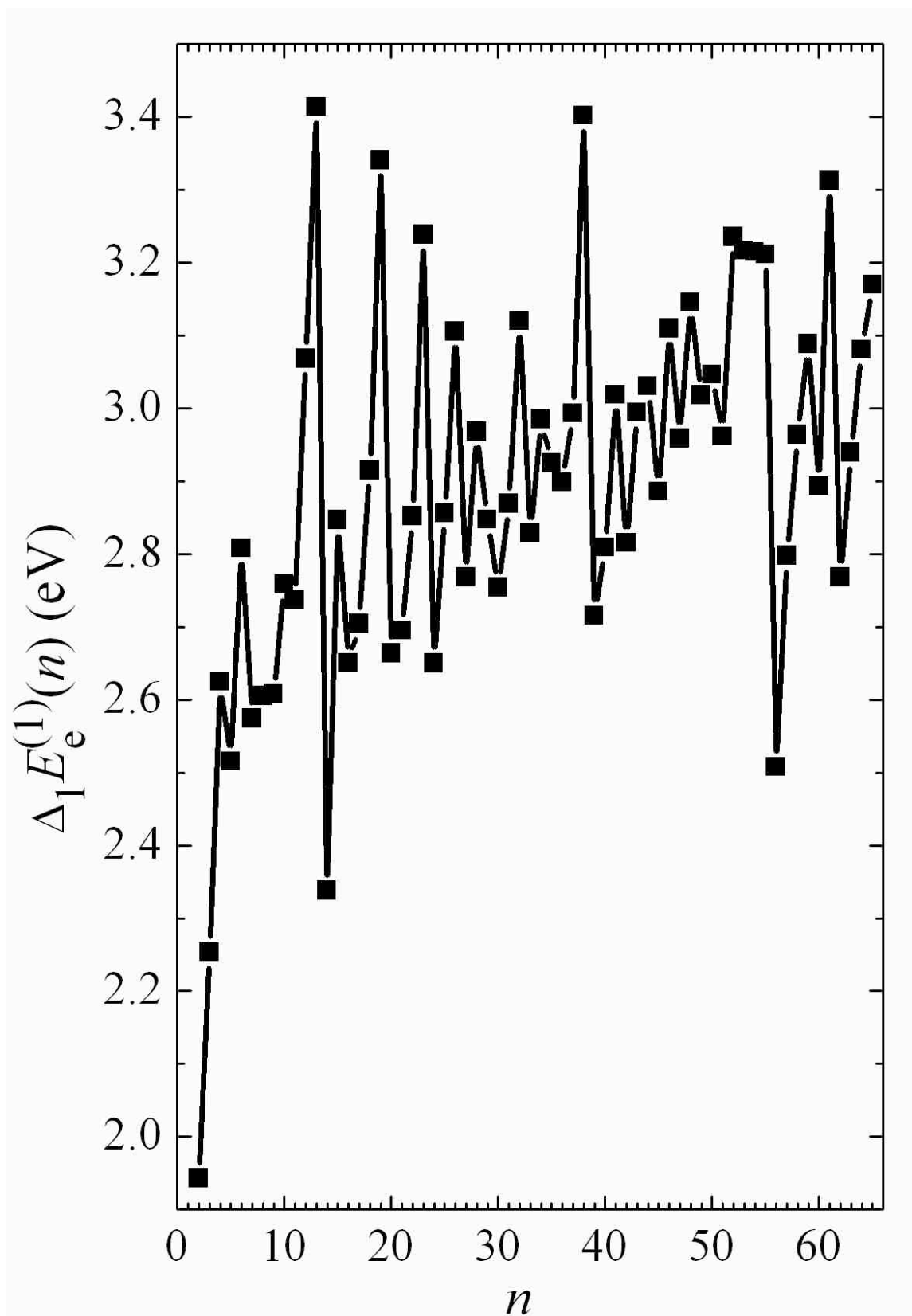


Fig. S3(a)

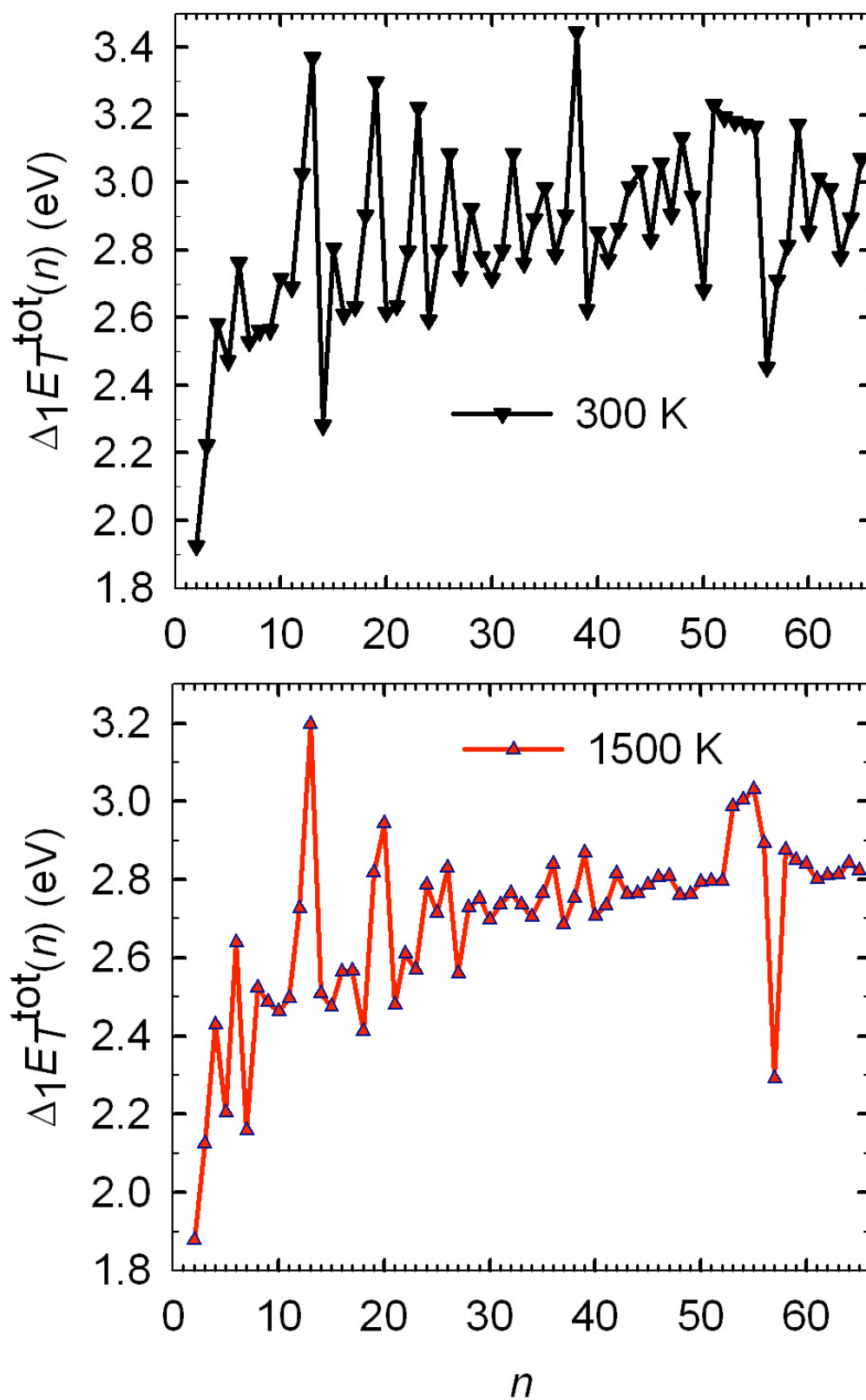


Fig. S3(b)

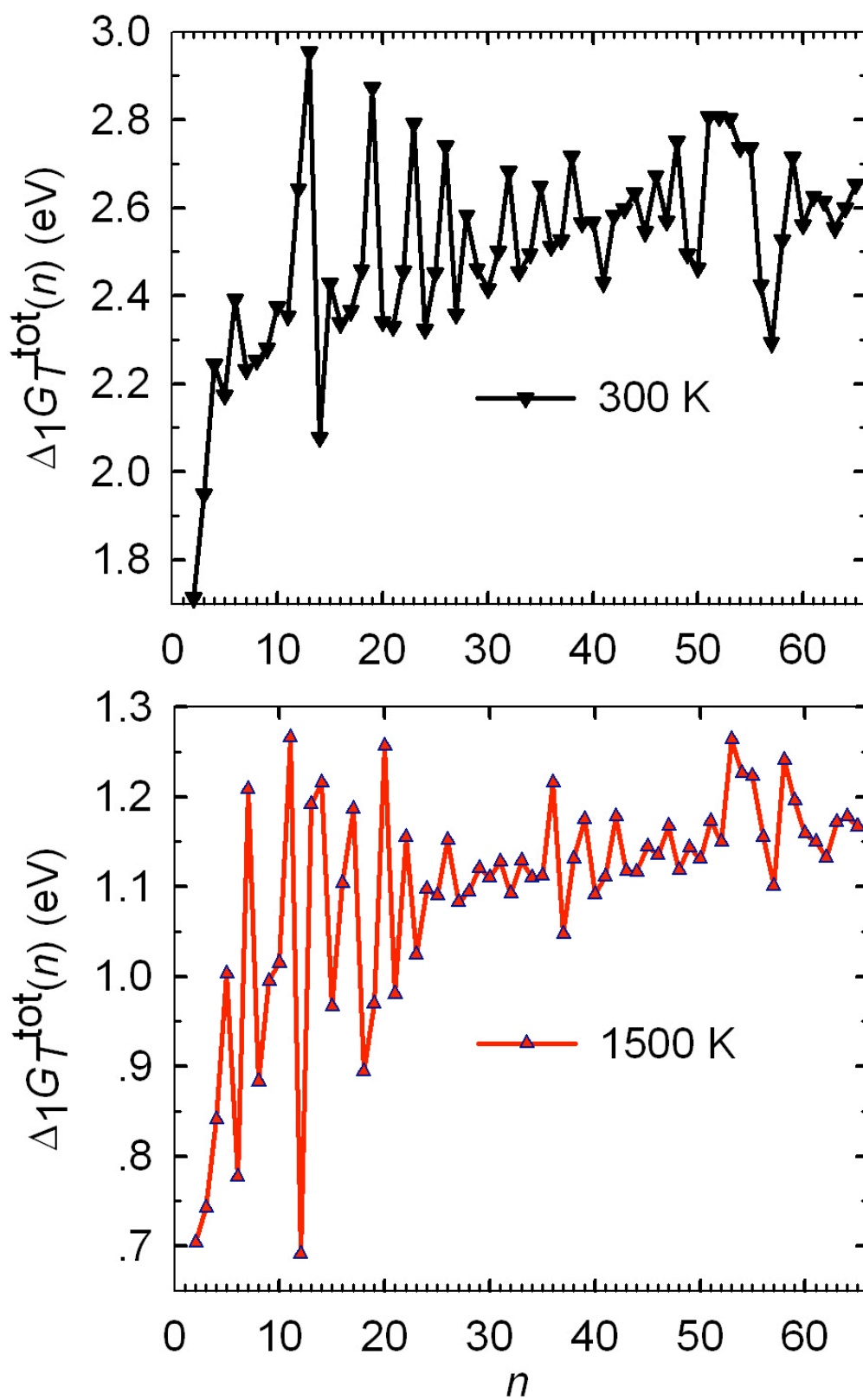


Fig. S3(c)

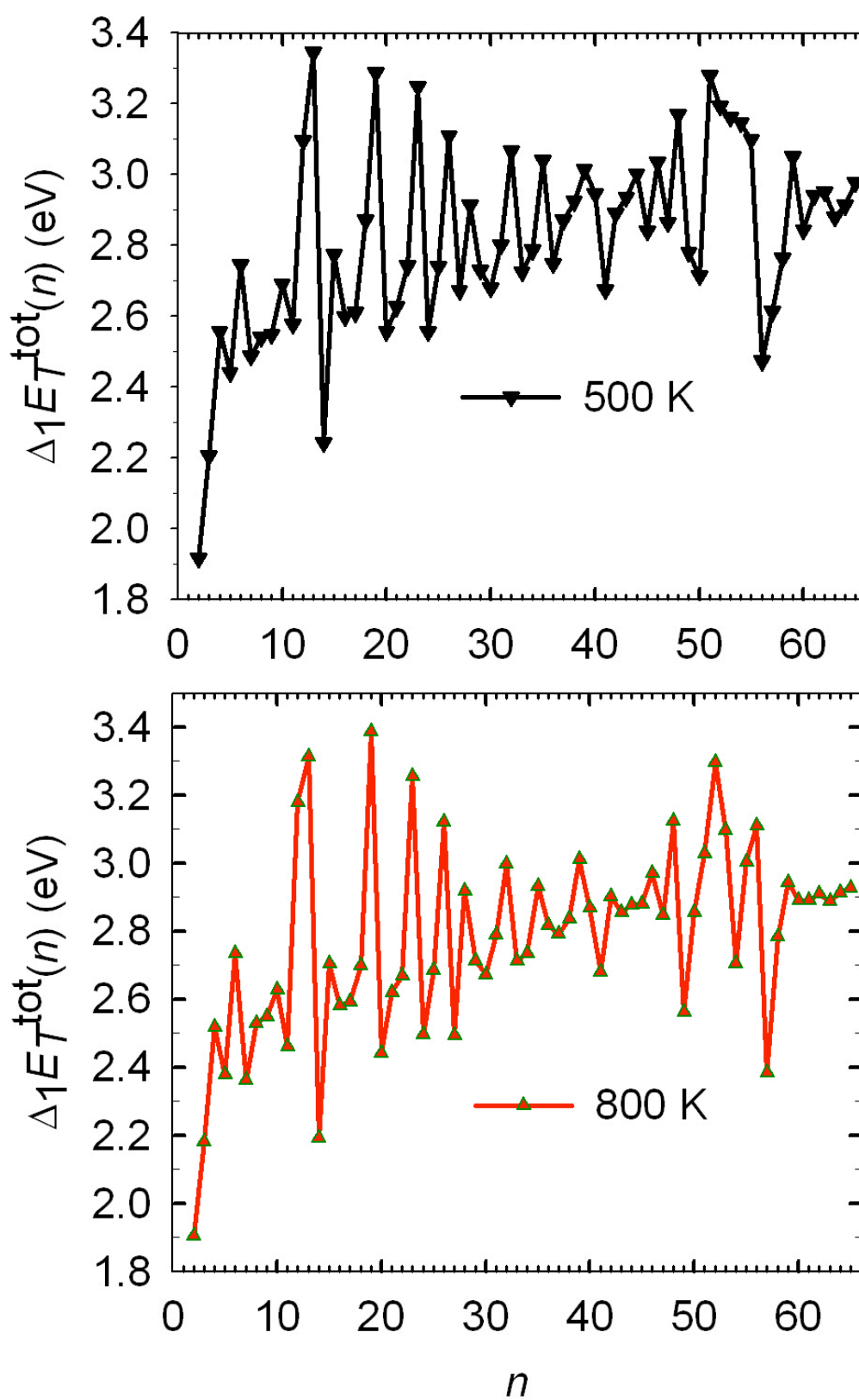


Fig. S4(a)

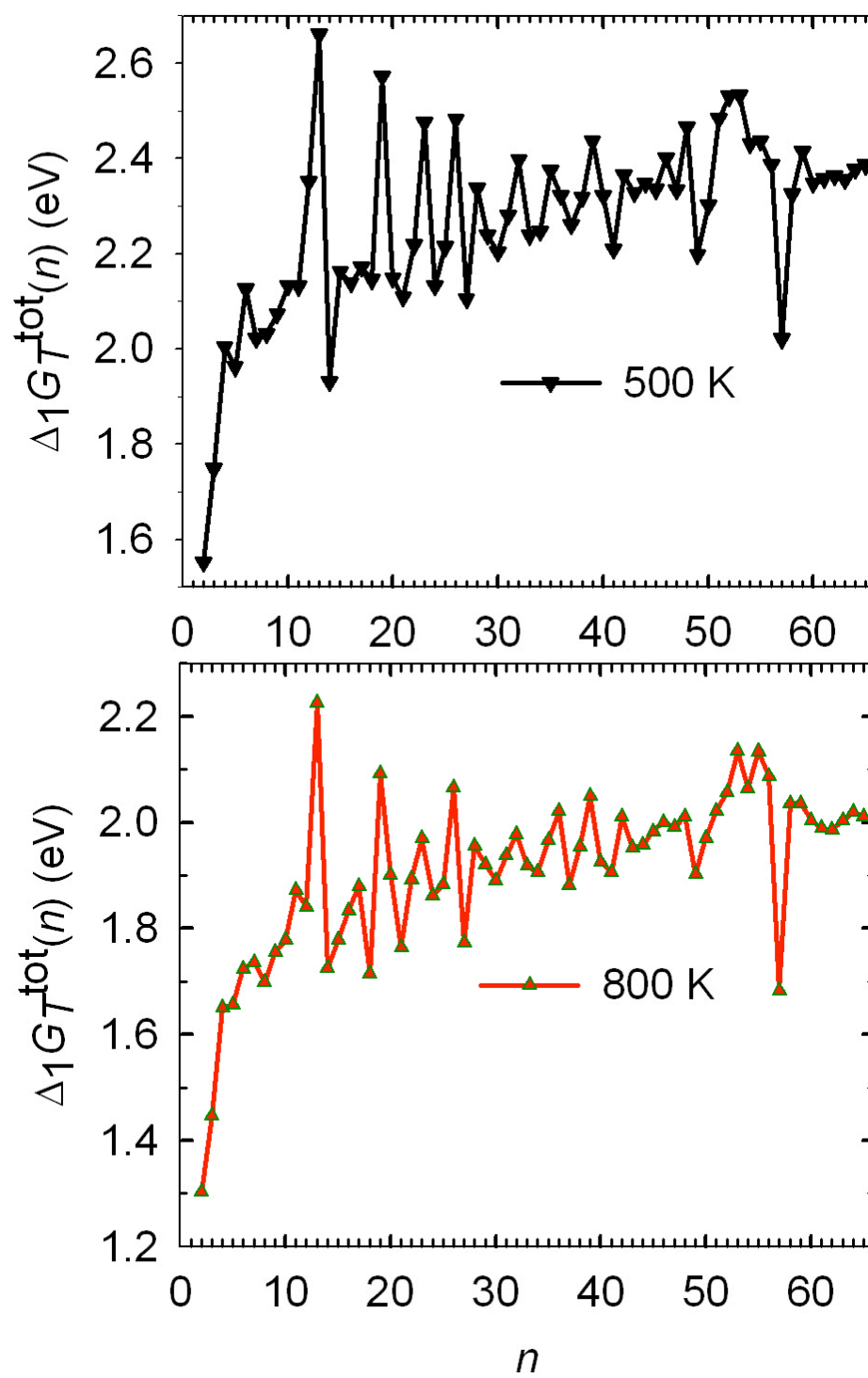


Fig. S4(b)

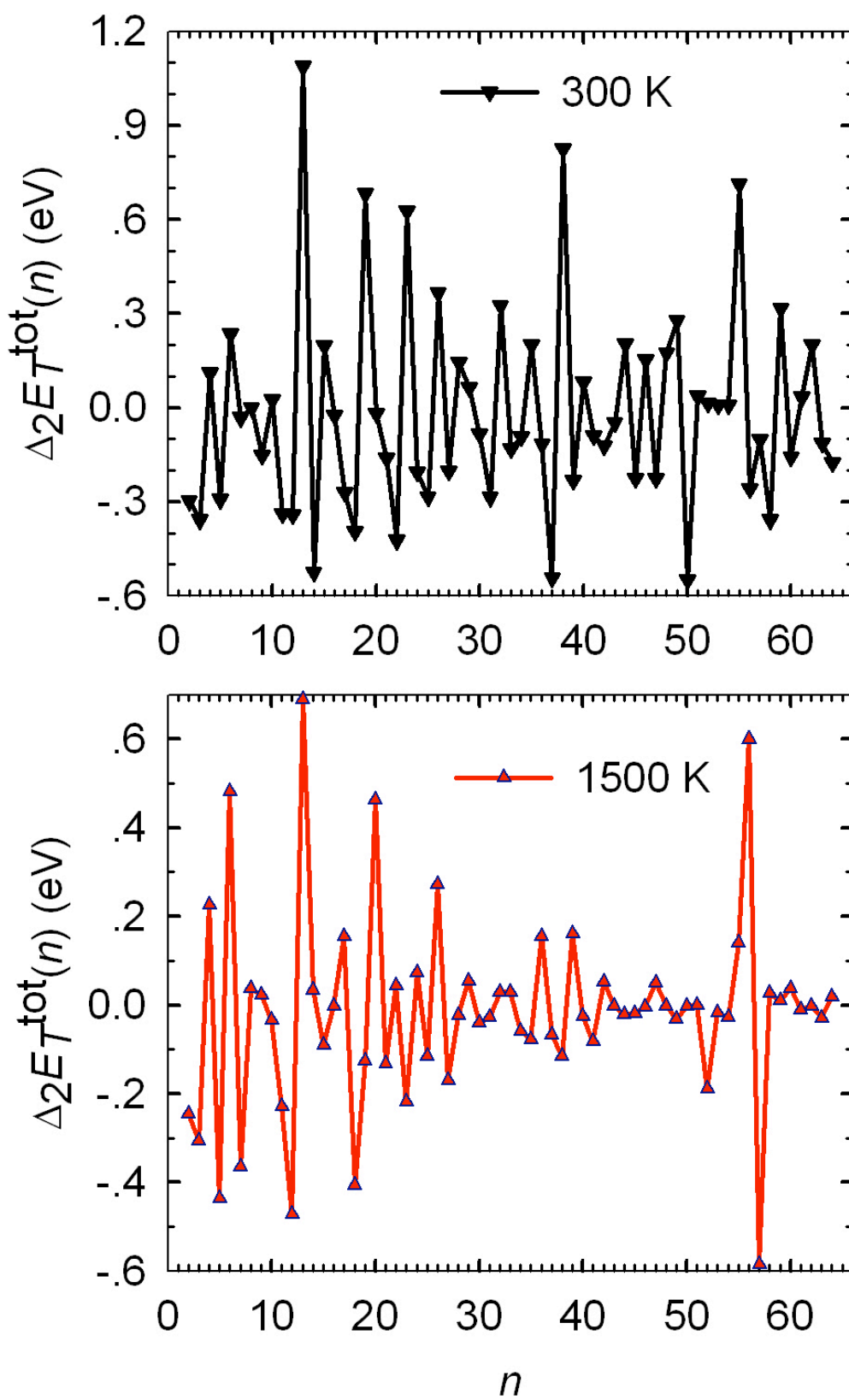


Fig. S5

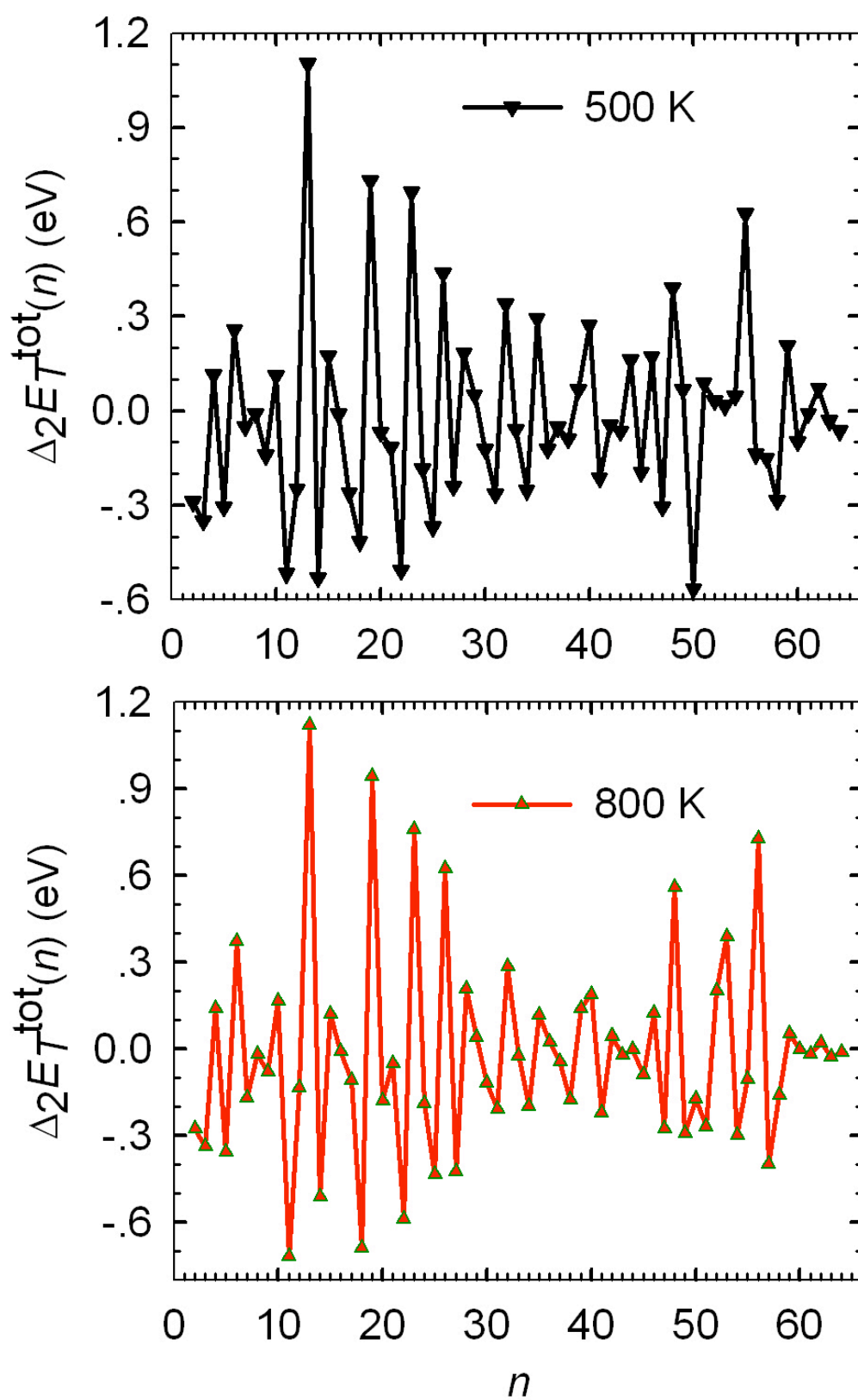


Fig. S6(a)

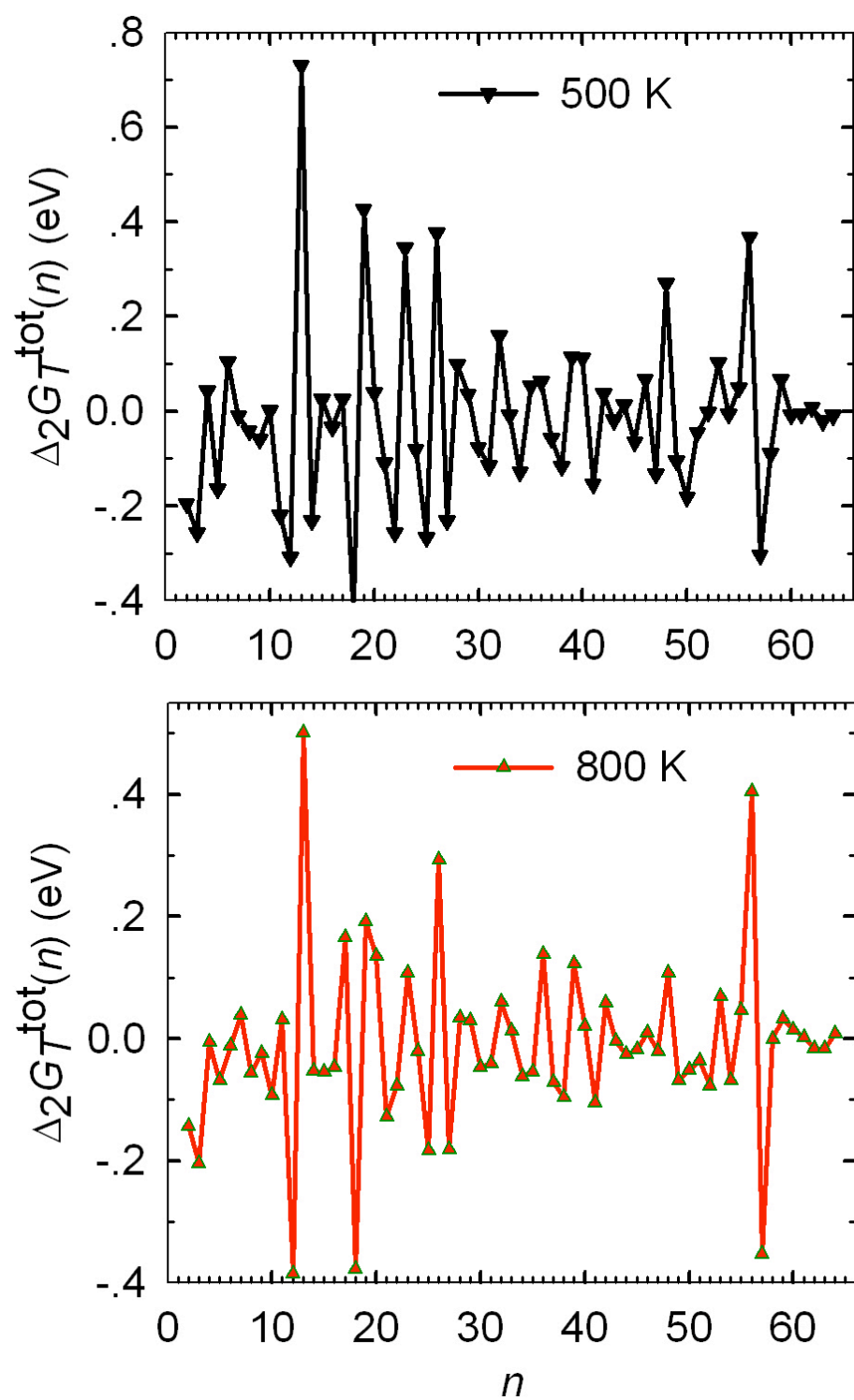


Fig. S6(b)



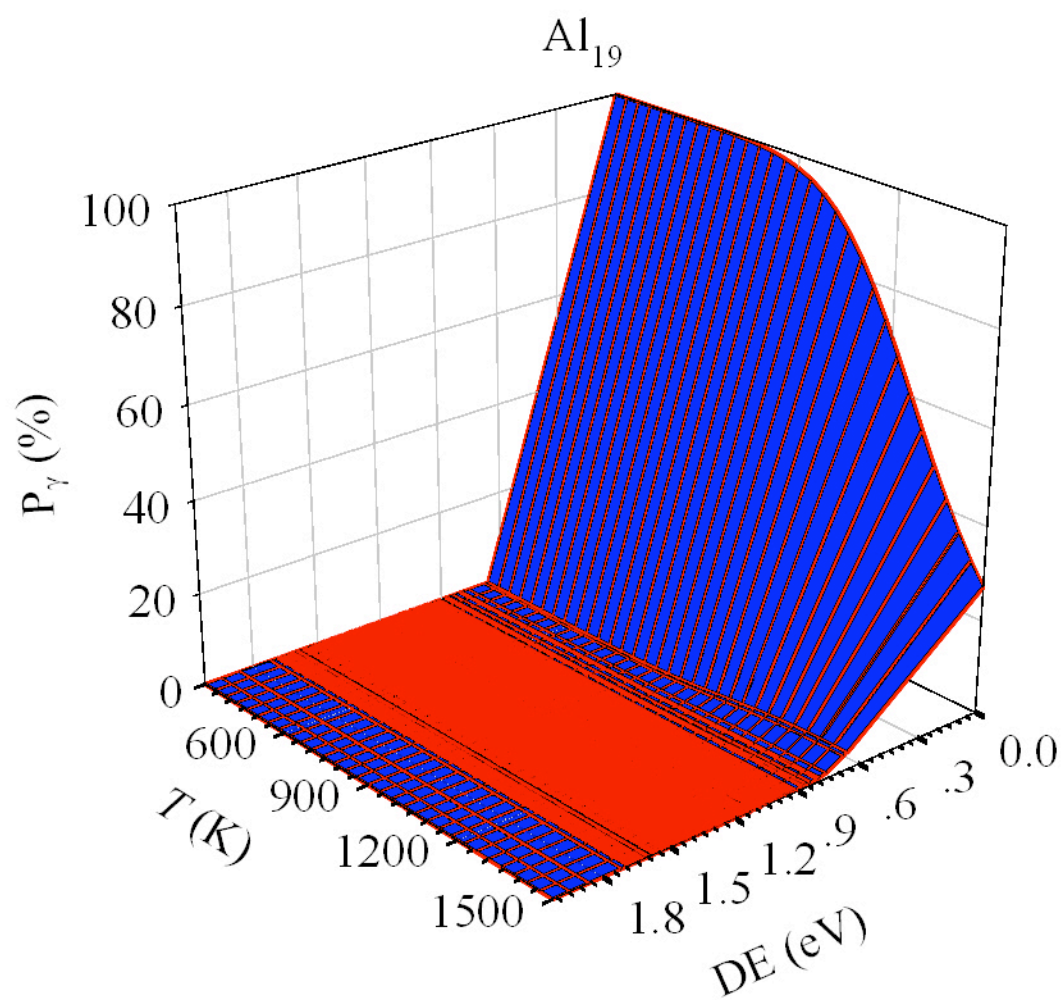


Fig. S7(b)

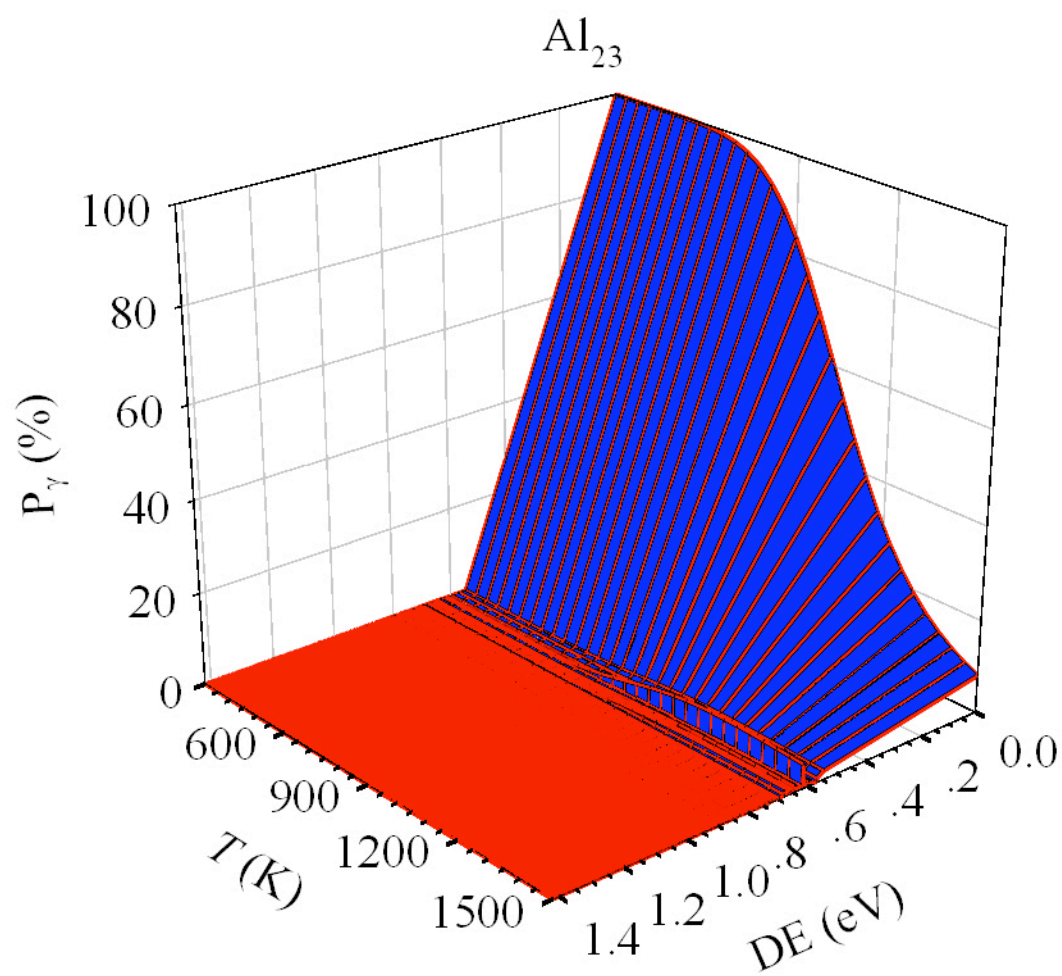


Fig. S7(c)

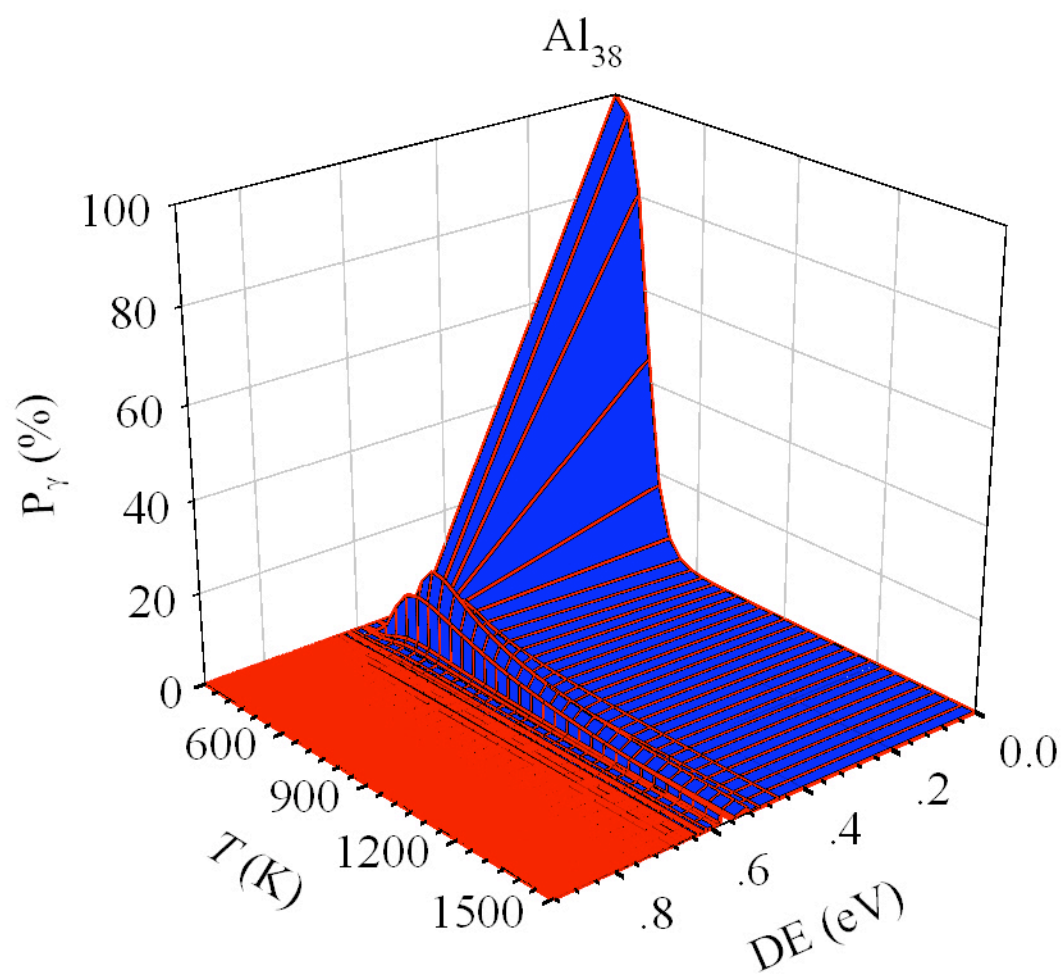


Fig. S7(d)

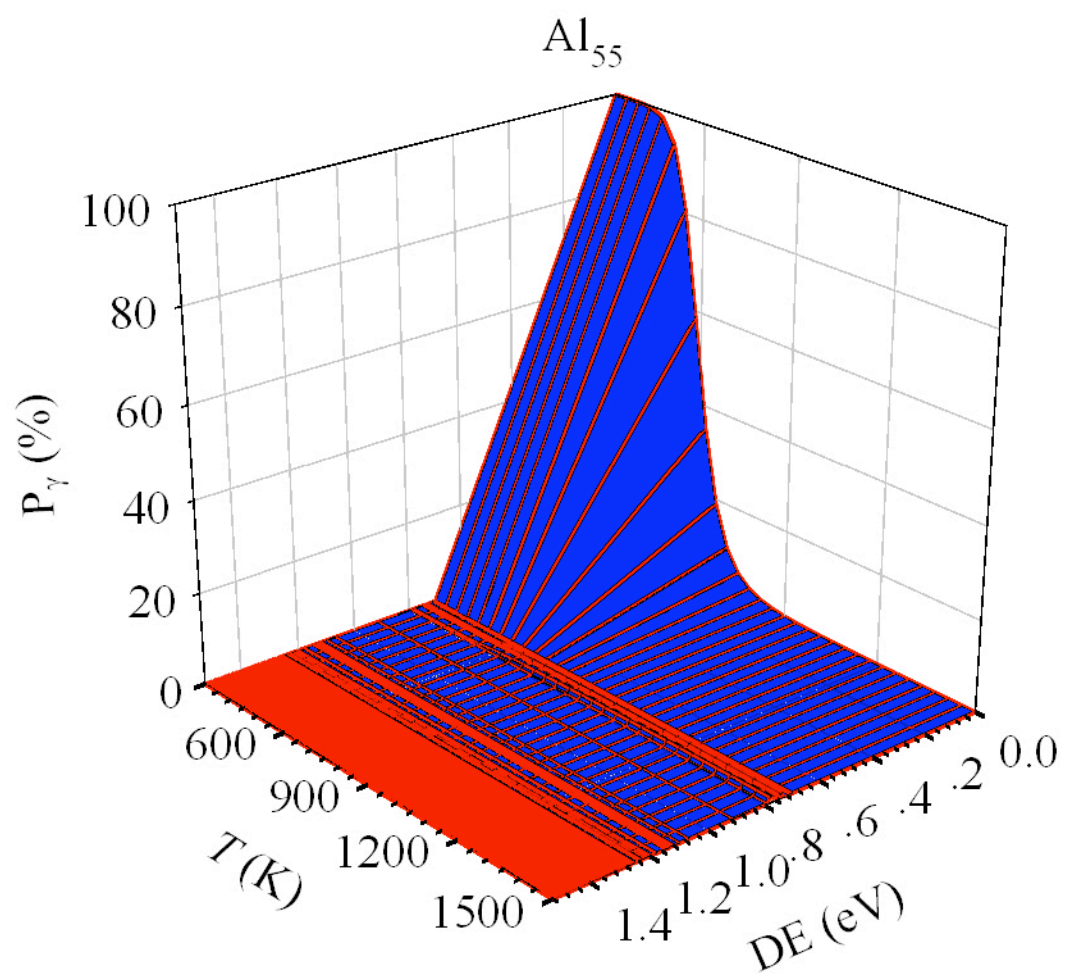


Fig. S7(e)

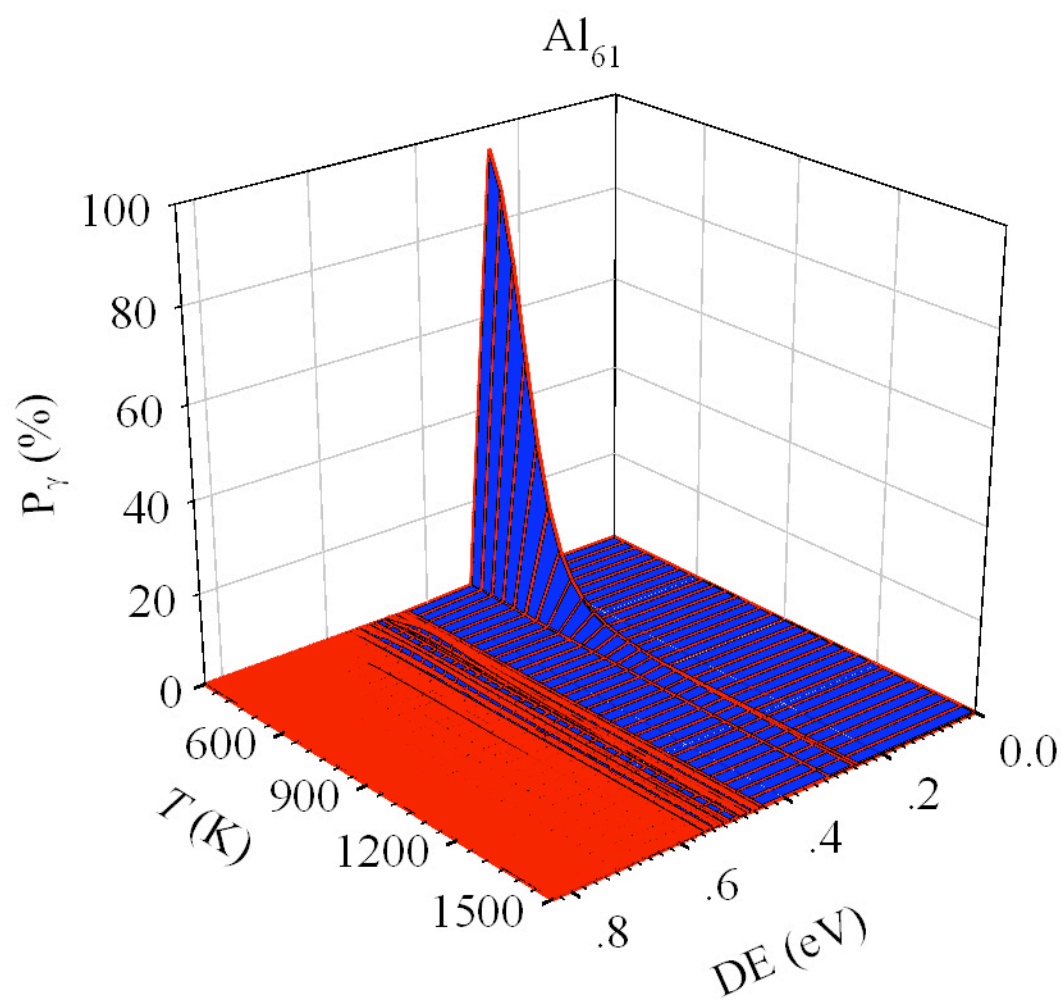


Fig. S7(f)

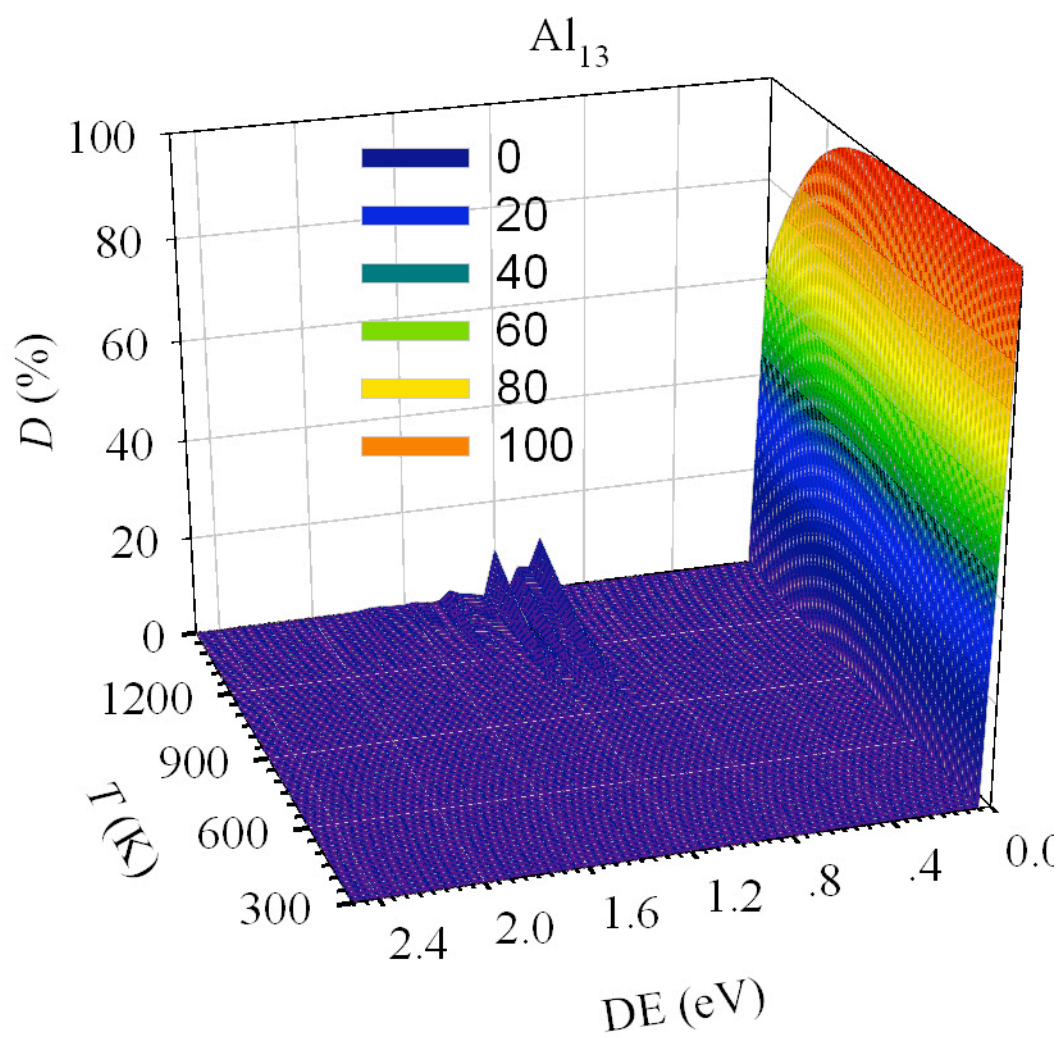


Fig. S8(a)

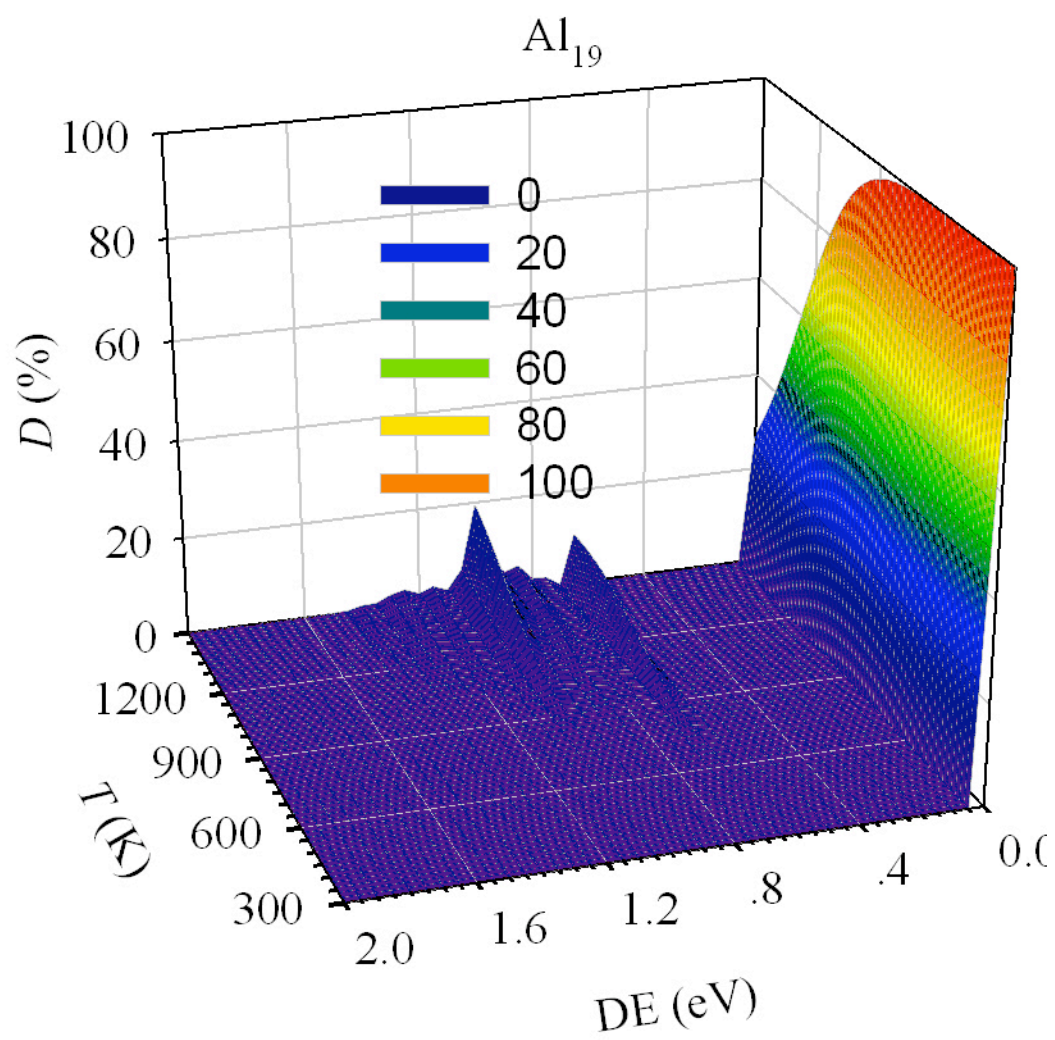


Fig. S8(b)

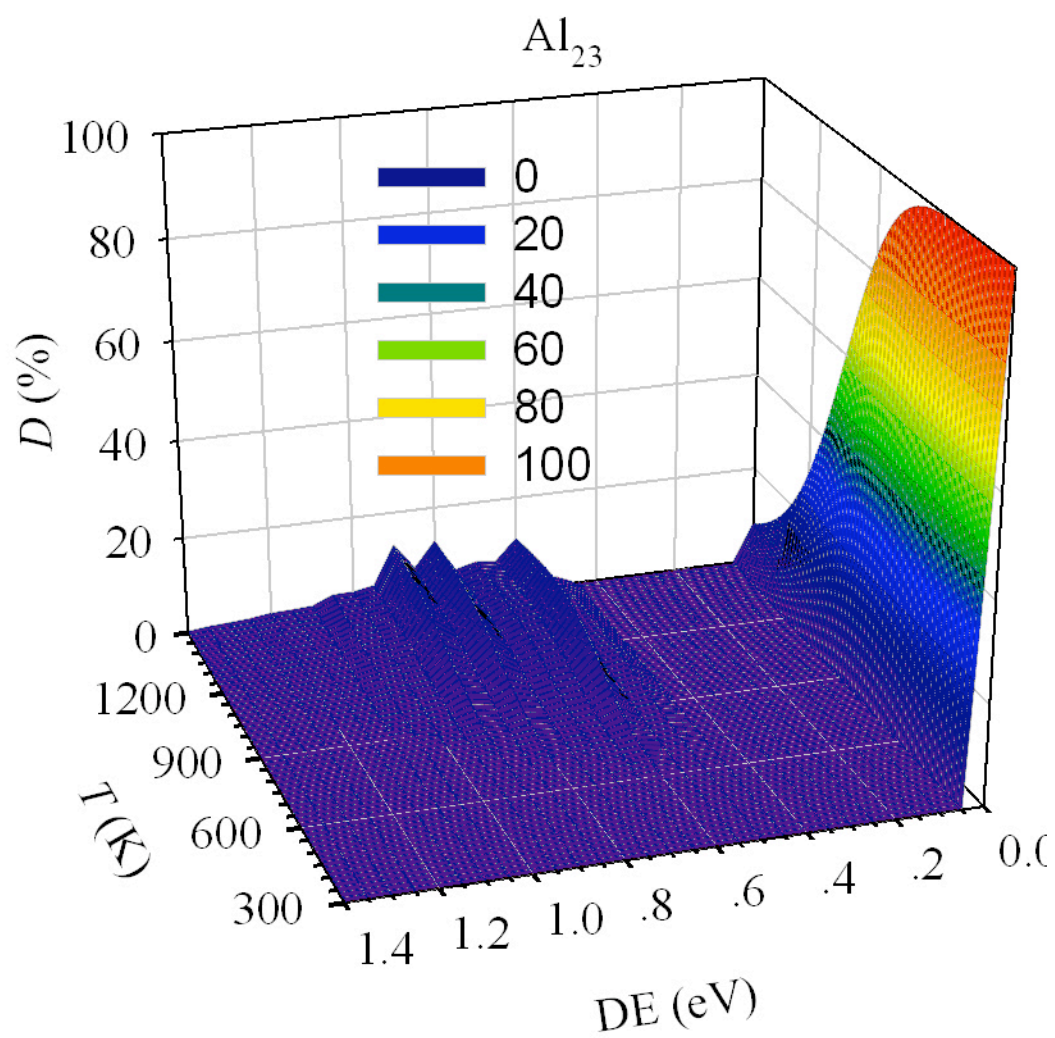


Fig. S8(c)

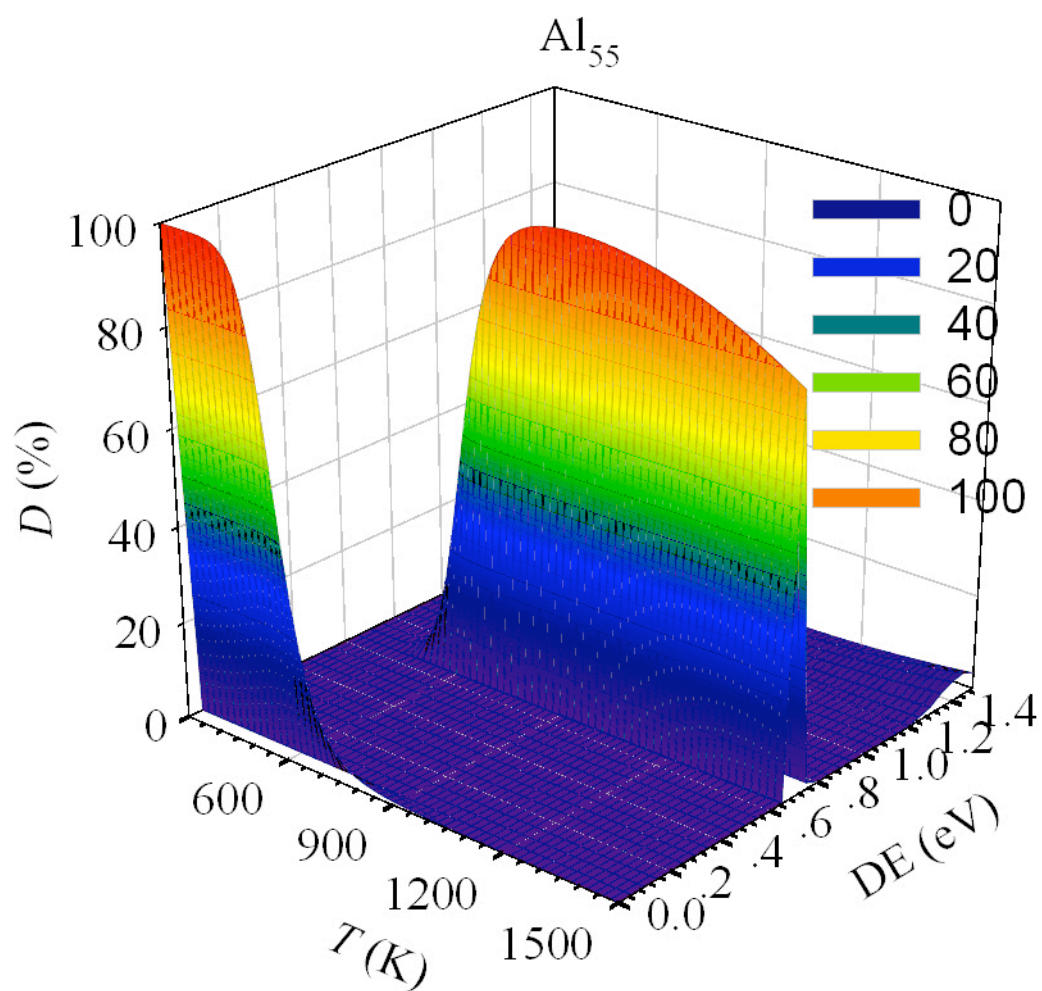


Fig. S8(d)

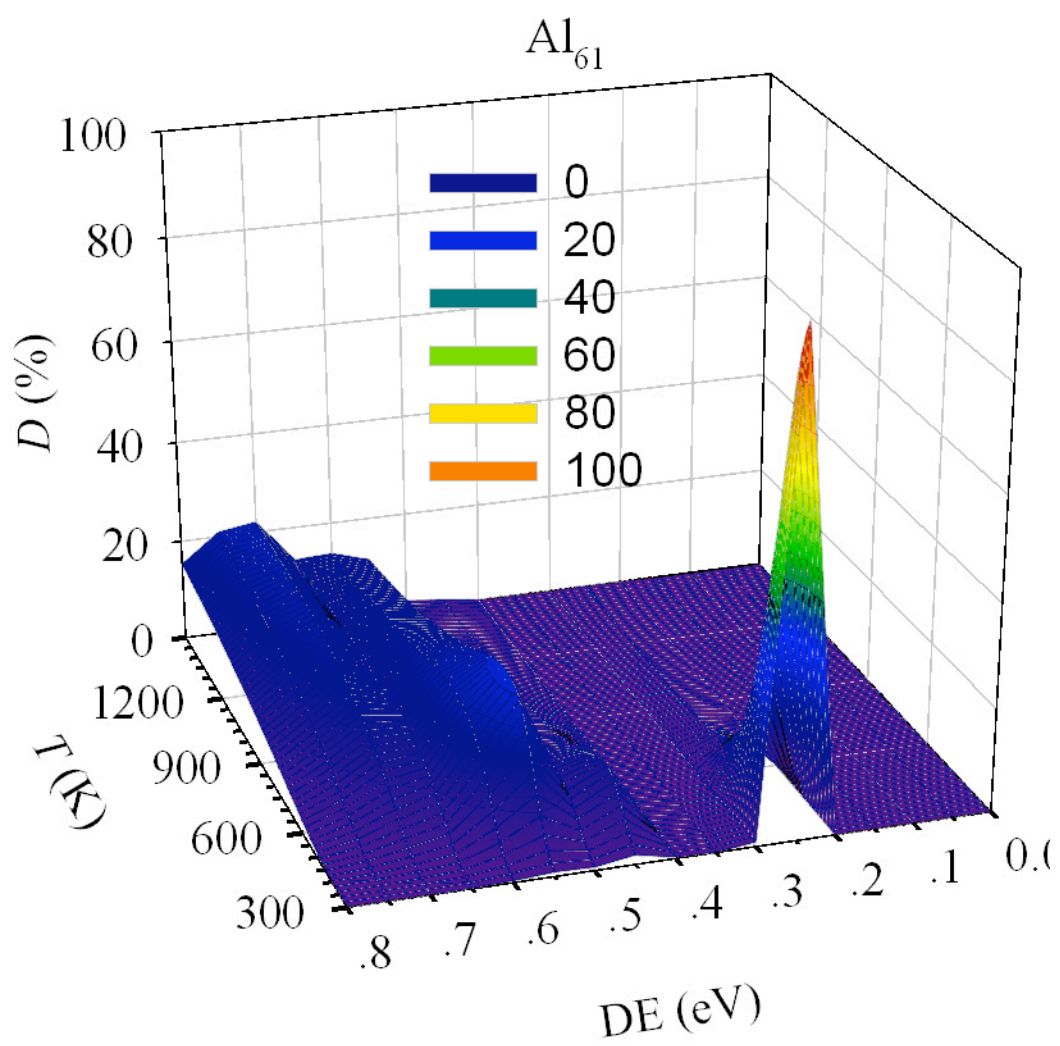


Fig. S8(e)